We are IntechOpen, the world's leading publisher of Open Access books
Built by scientists, for scientists

6,900
Open access books available

185,000
International authors and editors

200M
Downloads

154
Countries delivered to

Our authors are among the

TOP 1%
most cited scientists

12.2%
Contributors from top 500 universities

CLARIVATE ANALYTICS
BOOK CITATION INDEX
INDEXED

WEB OF SCIENCE™

Selection of our books indexed in the Book Citation Index
in Web of Science™ Core Collection (BKCI)

Interested in publishing with us?
Contact book.department@intechopen.com

Numbers displayed above are based on latest data collected.
For more information visit www.intechopen.com

Microgravity and Its Applications in Geosciences

Hakim Saibi

Abstract

Gravity is the most important force which determines the structure and evolution of stars like the Sun as well as the structure and evolution of galaxies. The law of universal gravitation is generally sufficient to describe the gravity of the Earth, the Moon, or the planets orbiting the Sun. With the recent development of sensitive gravimeters, the gravity survey has become one of the most used geophysical tools in applied geosciences for tasks including: exploring for oil and gas fields by studying geological structures and salt dome intrusion, monitoring groundwater and geothermal reservoirs by determining recharge and discharge masses, monitoring volcanic activity and hydrothermal activity beneath volcanoes, monitoring CO_2 movement during and after sequestration, locating active faults responsible for big earthquakes, and also exploring mines and detecting local cavities. In this chapter, we present a brief introduction to gravity and Bouguer gravity, the different corrections applied to measured gravity and follow with cases of applied microgravity measurements in different fields of geosciences.

Keywords: gravity, faults, geological structures, volcanoes, groundwater, geoscience

1. Introduction

The gravity method is a nondestructive geophysical technique that measures differences in the Earth's gravitational field between specific locations. It has many applications in engineering and environmental studies such as locating karsts, monitoring aquifer recharge, determining geologic layer thickness and the structure of the basement rocks, estimating the mass and volume changes in geothermal reservoirs, monitoring precursors of volcanic eruptions, and monitoring gas production and carbon sequestration. The gravity method is also used in oil, gas, and mineral exploration.

INTECH

open science | open minds

The gravity method depends mainly on the differences in the density of the Earth materials. The variations of densities of subsurface rocks produce variations in the measured gravity field. There are many numerical and analytical methods to study the variations in gravity and interpret the source of these variations (geometry, depth, and density). A GPS measurement should be associated with gravity measurements in order to know the exact coordinates (longitude and latitude) of the gravity stations and their altitudes. The measured gravity data is then processed by removing all the quantifiable disturbing effects and interpreted using computer programs. The most highly processed data are known as the Bouguer gravity, and anomalies are measured in units of mGal. Recent computer models are capable of creating three-dimensional subsurface density models.

2. Gravity method

2.1. Definition of the gravity field

The gravity field is defined as follows: a gravitational force or gravity exerted on a unit mass at a point in space or on the surface of the earth or its vicinity [1]. The gravity field is a force or a force field distributed over the region surrounding the generator. A measurement of gravity fields should be made in a region or space in which gravity fields exist.

2.2. Gravity method and its applications

Gravity is a geophysical potential field method. Various applications and developments of gravity method in the fields of geology, engineering, geothermal, and volcanology have been demonstrated and developed. Gravity can be used in time-series applications such as geothermal reservoirs and by estimating the underground mass changes [2, 3]. Also, gravimetric studies at active volcanic systems have contributed significantly to the better understanding of pre-, syn-, and post-eruptive processes [4, 5]. With the development of gravimeters with improved accuracy, the measurements have become much easier. Recently, time-variable gravity from satellites has detected the redistribution of mass over large scales and the gravity data are used, for example, in hydrology and oceanography. The gravity method can also detect geological anomalies and contacts (faults) by using gravity gradient interpretation techniques.

2.3. Basics of gravity

Gravity surveying is based on Isaac Newton's universal law of gravitation, described in *Principia Mathematica* in 1687. One of the basic forces of nature is the attraction between all masses. This attraction is called the force of gravity. According to the Newtonian law of gravity, the gravitational force between any two point masses is given by:

$$F = \frac{G\ M_1\ M_2}{r^2} = gm \tag{1}$$

where G (universal gravitational constant) = 6.673×10^{-11} m³ kg⁻¹ s⁻². M_1 and M_2 are the two masses in kg, and r is the distance between the point masses, in meters. g is the local value of the Earth's field, and m is a test mass. This force acts in the direction joining the two masses (**Figure 1**). **Figure 2** shows the gravitational attraction of a small mass on the Earth.

2.3.1. Units of gravity

Recent gravity meters are very sensitive and can routinely measure differences in the gravity field to within one part in 10^9. The c.g.s unit commonly used in gravity measurement is the milliGal: 1 mGal = 10^{-3} Gal = 10^{-3} cm s⁻². In gravity surveys, commonly, mGal is used.

2.3.2. Shape of the Earth

If the Earth was a uniform, homogenous sphere, g would be constant over its surface. However, gravity varies because the density varies within the Earth, and the Earth is not a perfect sphere. One predictable effect on local gravity measurements is earth's shape. The Earth has the shape of a flattened sphere because of its rotation (**Figures 3–5**).

2.4. The pendulum

It is possible to find the acceleration of gravity (g) from the period of oscillation of a pendulum (**Figure 6**) swinging with a small amplitude using Eq. (2):

$$g = (2\pi f)^2 L \tag{2}$$

where f is the frequency and L is the length.

2.5. Modern gravimeters

There are two main types of modern gravimeters. The first type, which uses a pendulum arrangement or a dropping weight, records the actual acceleration of gravity wherever it is placed. The second type uses levers and springs to measure the difference in gravity between two stations. Since the springs are not calibrated, these readings are all relative to a base station.

Gravimeters, essentially a mass suspended from a sophisticated spring balance, have been used to measure relative gravity since 1930s. As weight of mass (mass x gravity) increases, the spring is stretched (**Figure 7**).

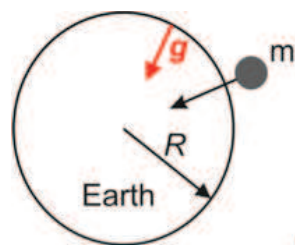

Figure 1. Attractive force acting between two bodies.

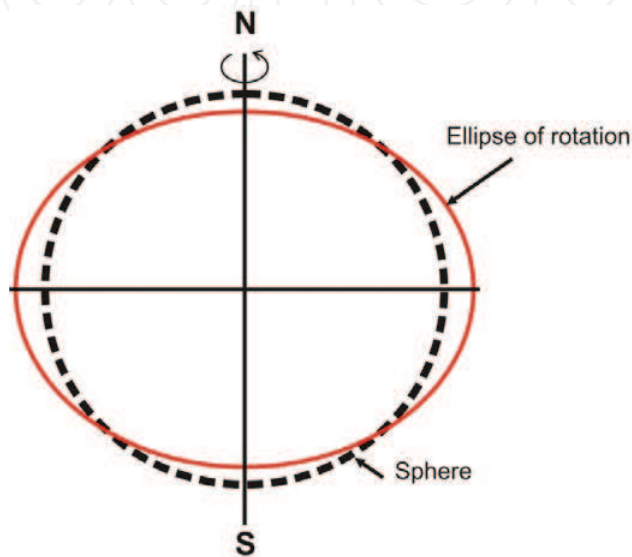**Figure 2.** The gravitational attraction of a small mass m on the Earth.

Figure 3. Exaggerated difference between a sphere and an ellipse of rotation (spheroid).
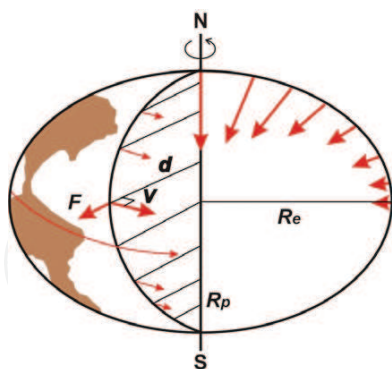

Figure 4. Centrifugal acceleration and variation of gravity with latitude ϕ (not to scale). The gravity is 5186 mGal greater at the poles than at the equator. The acceleration due to gravity varies with latitude due to two effects: The Earth's shape and the Earth's rotation [6].

2.5.1. Relative modern gravimeter

2.5.1.1. CG-3M relative gravimeter

The Scintrex CG-3M gravimeter is a very sensitive mechanical balance that detects gravity field changes as small as one part in a million. CG-3M (**Figure 8**) has a resolution of 1 μGal
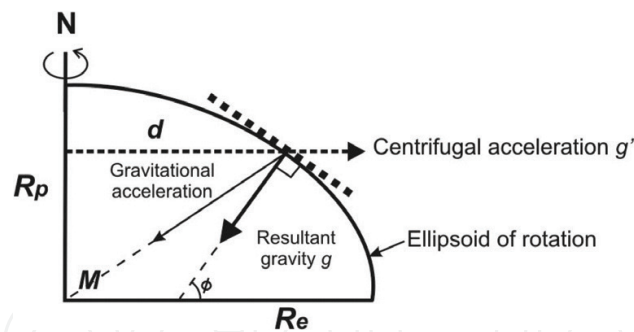
Figure 5. Resultant of centrifugal acceleration (g') and the acceleration due to gravity (g) [6].
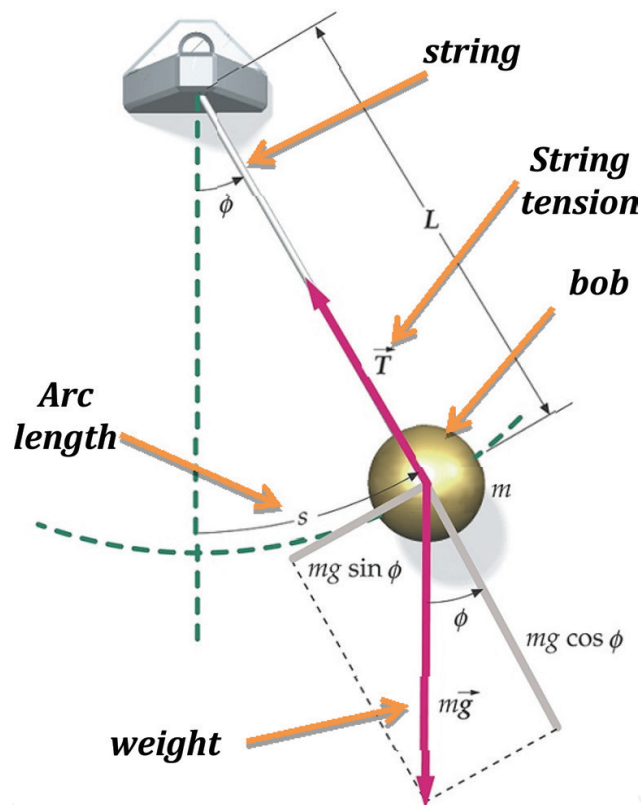

Figure 6. The pendulum.

and automated corrections for tide, instrument tilt, temperature, and rejection of noisy data. **Figures 9** and **10** show the CG-3M gravimeter in the field with GPS measurement. Please check **Table A1** for gravity data sheet information.

2.5.1.2. CG-6 relative gravimeter

The CG-6 Autograv (Scintrex) is the newest generation of land gravity meter. **Figure 11** shows CG-6 acquired by United Arab Emirates University in March 2017. **Figure 12** shows the gravity stations observed in Al Ain city. **Figure 13** shows the three-dimensional inversion of the Bouguer gravity data for geological investigations.
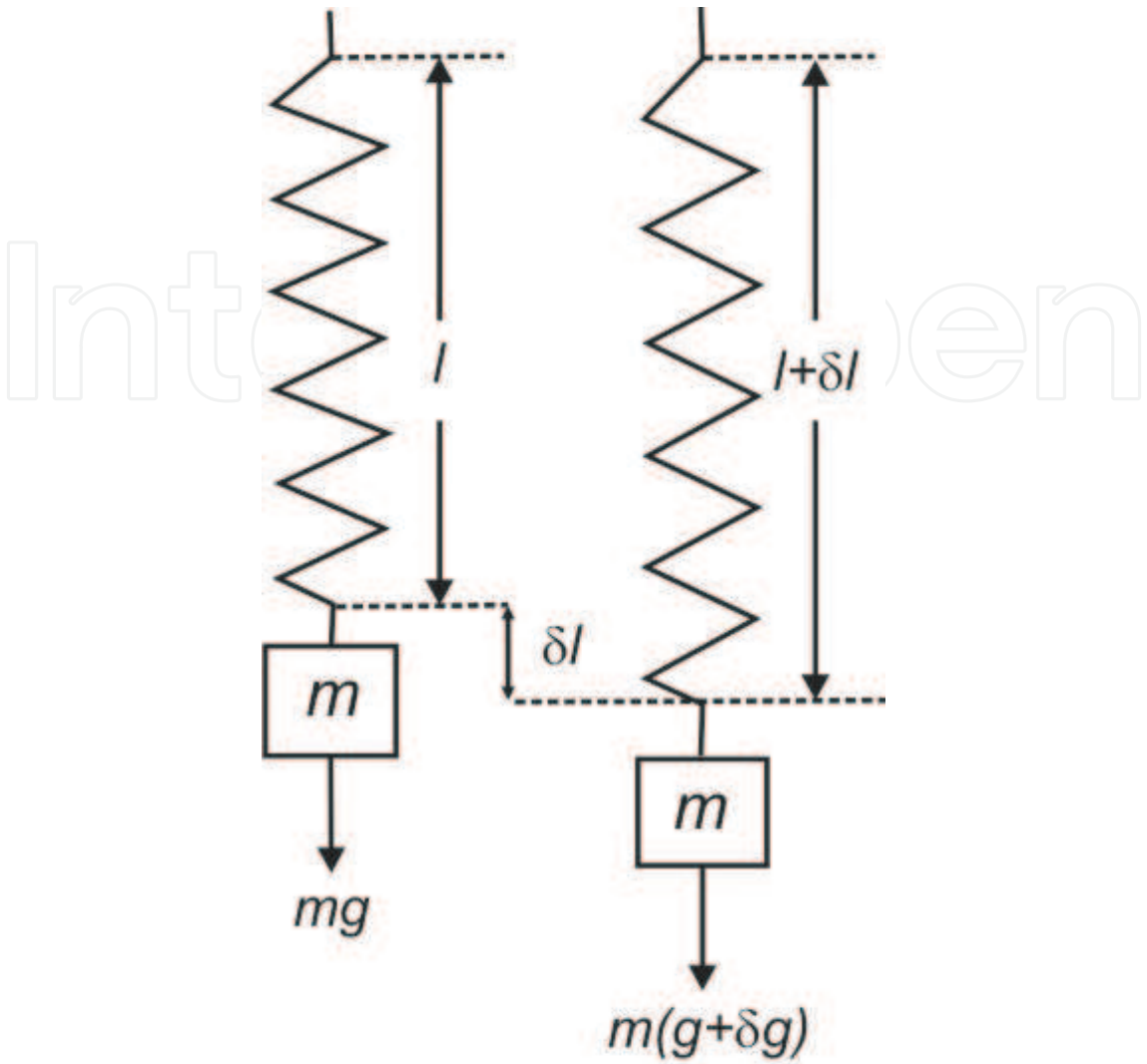
Figure 7. Extension (δl) of a spring due to additional gravitational pull (δg).
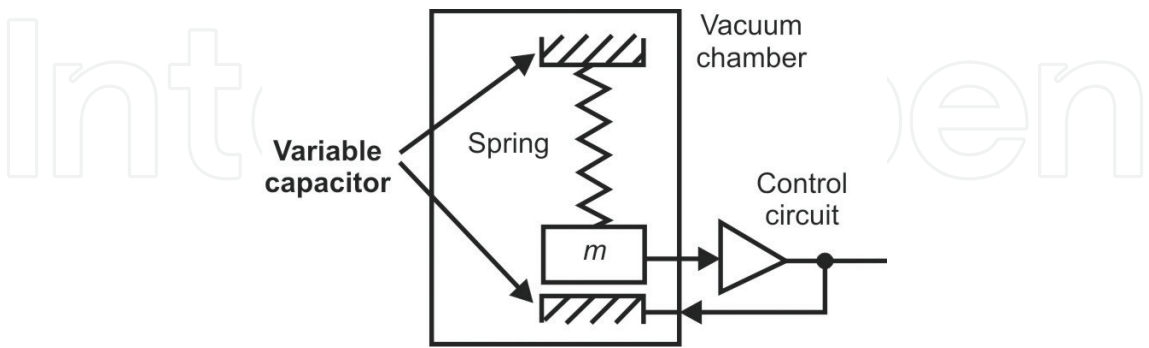

Figure 8. Scintrex CG-3 gravimeter.

2.5.2. Absolute modern gravimeter

The A-10 (**Figure 14**) is a portable absolute gravimeter recently developed by Micro-g LaCoste, Inc. (MGL) that is designed for use in the field to measure the vertical acceleration of gravity (g).
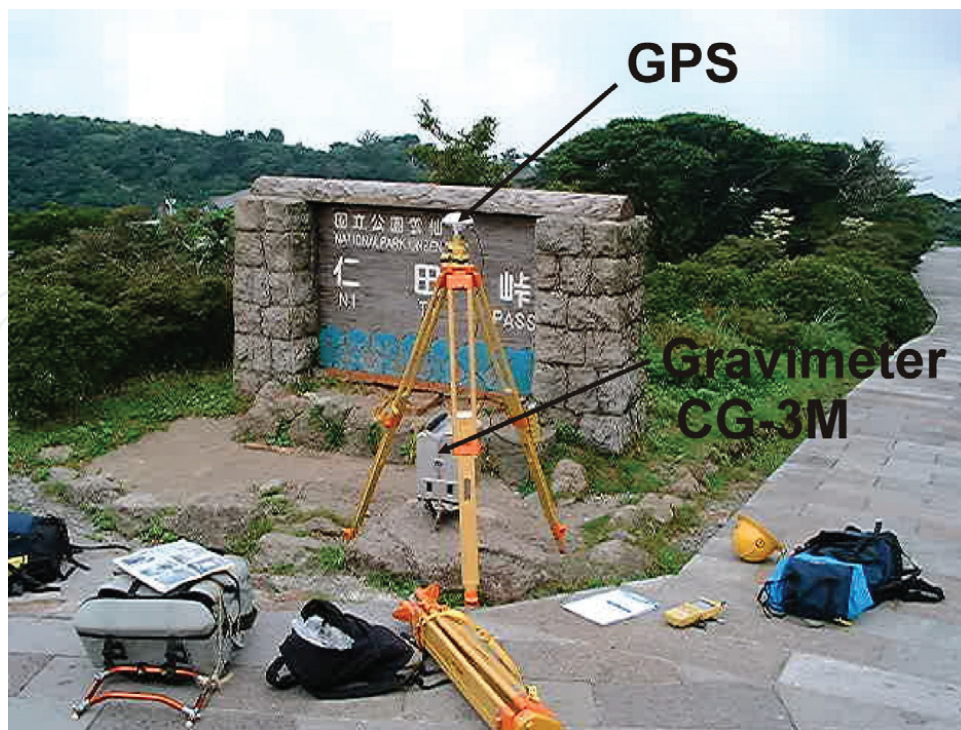
Figure 9. Photograph showing the Scintrex CG-3M gravimeter and GPS antenna at Nita station (Unzen volcano, southwestern Japan) [7].

Figure 10. Photograph of CG-3M Autograv automated gravity meter. The features of this gravimeter are: resolution mGal = 0.001 (=1 μGal), standard deviation: <5 μGal, automated corrections: tide, instrument tilt, temperature, and rejection [7].

Figure 11. Top view of CG-6 gravimeter during field measurement in Alain city, United Arab Emirates (June 2017) [7].

Figure 12. View of lynx LG software (Scintrex, 2017) showing the gravity stations in Alain city, United Arab Emirates, during field survey in Al-Ain city in June 2017. Lynx LG software includes data pre- and postprocessing that helps users to get a simple Bouguer gravity map of the study area just after finishing the measurements [7].

A test mass is dropped numerous times in a vacuum, and its position is measured with a laser interferometer as a function of time with an atomic clock. The vertical acceleration of gravity is calculated by fitting the equation of motion to the measured trajectory of the test mass. The drops are combined into a "set" which typically consists of 100–200 drops. Multiple sets are
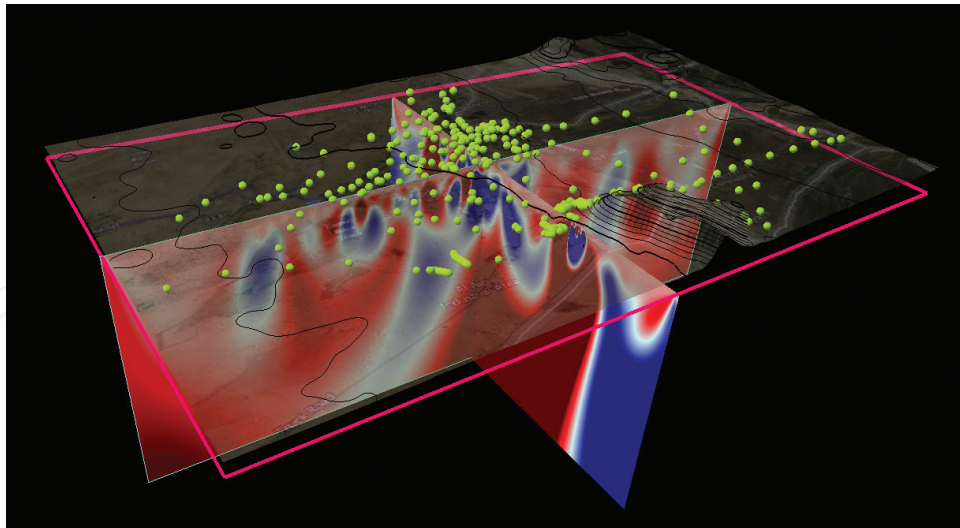
Figure 13. Three-dimensional gravity inversion of Alain city Bouguer gravity data using petrel gravity magnetic modeling and inversion plug-in (Schlumberger) showing regions of high and low densities beneath the study area [7].

Figure 14. Picture of A-10 absolute gravimeter.
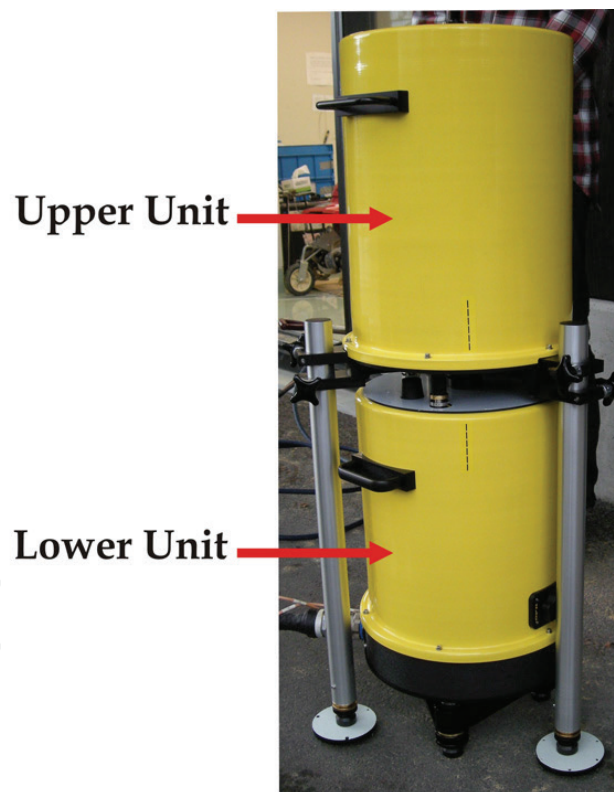
collected, and the average of the sets provides a value of g. The specifications of the A-10 are: a precision of 100 μGal at a quiet site, a repeatability of 10 μGal on a high-quality pier, and an accuracy of 10 μGal [8]. **Table 1** and **Figure 15** show the absolute gravity data recorded in Kyushu University [7]. Please check **Table B1** for gravity data sheet information.

Setup height	2.20 cm
Transfer height	100.00 cm
Actual height	74.00 cm
Gradient	−3.086 μGal/cm
Nominal air pressure	1004.27 mBar
Polar motion coord.[**]	−0.1049 "0.2862"
Measurement precision	0.94 μGal
Number of sets	10
Number of drops	100
Gravity	979634789.69 μGal

[**]The polar motion changes daily. From the MGL website, we can download the values of polar motion and enter them in the computer before processing the gravity data.

Table 1. Example of absolute gravity measurements using A10 absolute gravimeter [7].

Measurement of absolute gravity at base station is very important in calculating absolute gravity values at other stations as follows:

$$G_{abs} = G_{absB} + G_{obs} - G_B + G_H + G_T + G_D$$

G_{abs} : absolute gravity value at the station

G_{absB} : absolute gravity value at the base station

G_{obs} : measured value at the station (mgal converted)

G_B : measured value at the base station

G_H : instrument height correction value at the station

G_T : tide correction value at the station

G_D : drift correction value at the station

2.6. Corrections to gravity observations

2.6.1. Instrumental drift

Gravimeters are very sensitive instruments. Temperature changes and elastic creep in springs cause meter readings to change gradually with time even if the meter is never moved. Drift is monitored by taking repeated readings at the same station over the course of the day, perhaps every 1–2 h, to produce a drift curve (**Figure 16**). Instrument drift correction for each station can be estimated from drift curve.
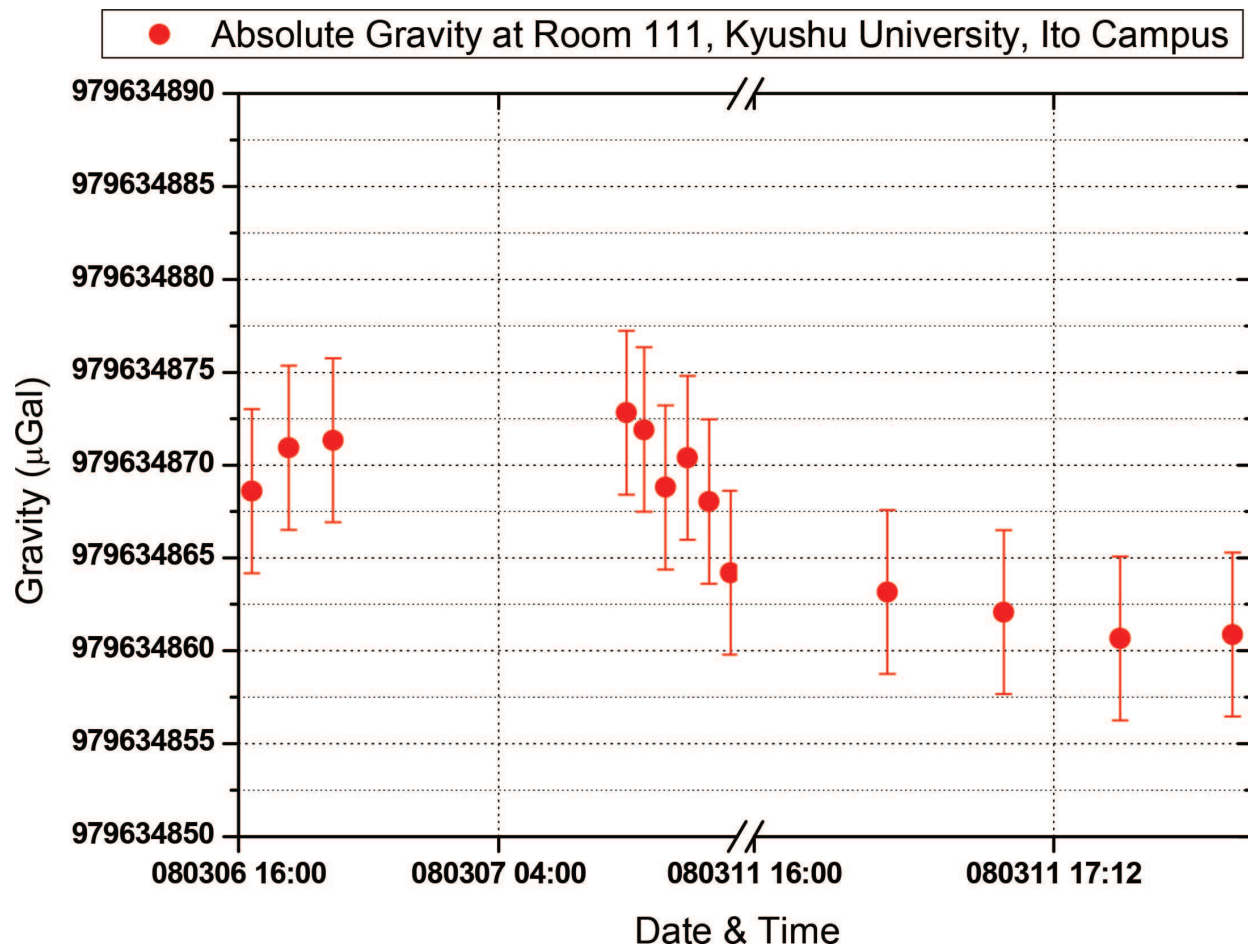
Figure 15. Change in absolute gravity measured by the absolute gravimeter A-10 at Kyushu University (Japan) after applying tidal, polar motion, and air pressure corrections. Measurement precision is 0.94 μGal; the number of sets is 10; the number of drops is 100. Analysis of the data indicates the instrument performed within the specifications of the manufacturer. The microgravity changes are associated with the shallow groundwater change due to rainfall [7].

2.6.2. Variation with elevation

2.6.2.1. Free-air effect

Height correction is important in a microgravity survey. The measured gravity is corrected by using free-air gradient of −308.6 μGal/m (**Figure 17**).

Free-air correction is the difference between gravity measured at sea level and at an elevation, h, as if there was no rock in between.

2.6.2.2. Bouguer effect

Free-air correction does not take into account the mass of rock between measurement station and sea level. The Bouguer correction, Δg_B, accounts for effect of the rock mass by calculating extra gravitational pull exerted by rock slab of thickness h and mean density ρ (**Figure 18**).
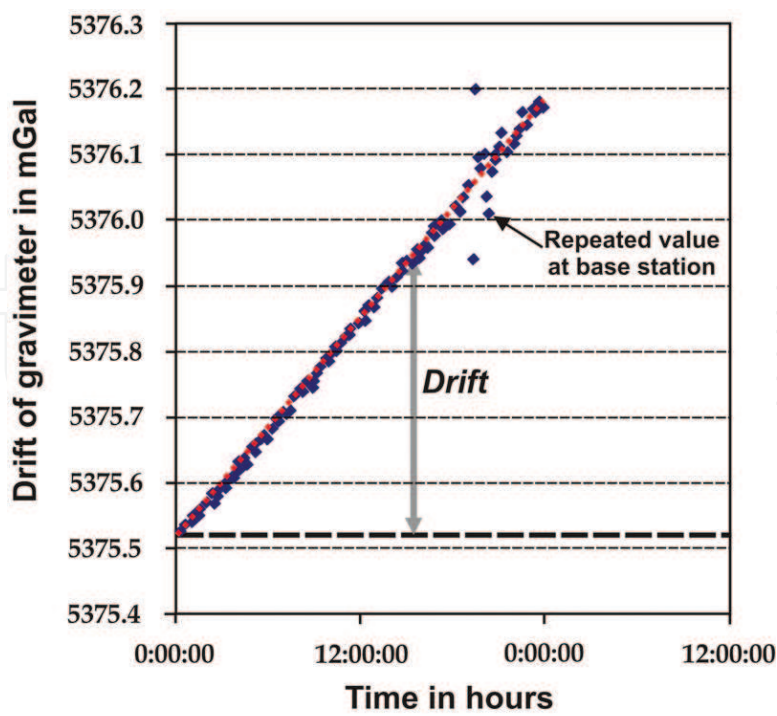
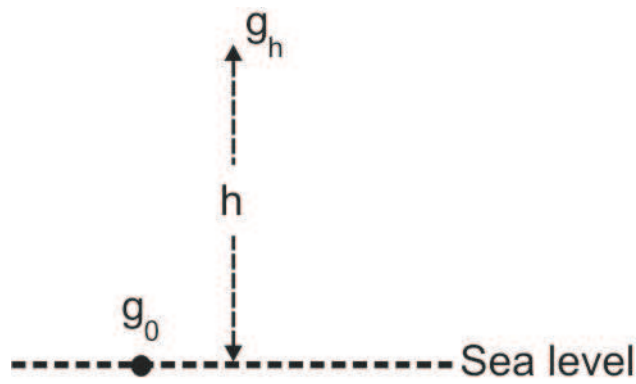**Figure 16.** An example of instrumental drift correction [7].

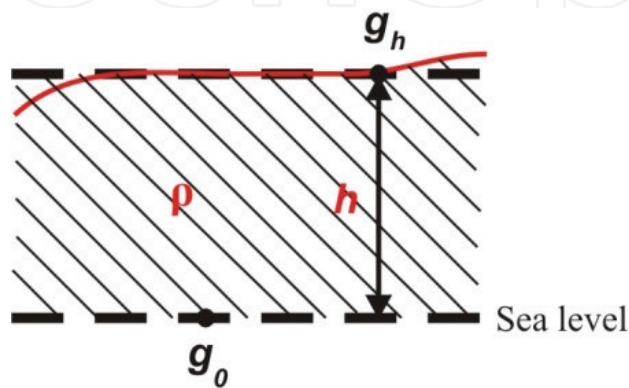

Figure 17. Free-air effect.

Figure 18. Bouguer effect.

$$\Delta g_B = +0.04192 \ h \ \rho \ \text{mgal} \tag{3}$$

2.6.2.3. Elevation effect

$$\Delta g_E = -(0.3086 - 0.0149\rho) \ \text{mgal/m} \tag{4}$$

2.6.2.4. Terrain effect

Bouguer correction assumes subdued topography. Additional terrain corrections must be applied where measurements are near to mountains or valleys (**Figures 19–21**). If the station is next to mountain, there is an upward force on the gravimeter from mountain that reduces the reading. This effect was first noticed in topographic surveys run near the Himalayan Mountains.

If gravity station is next to valley, there is an absence of the downward force on gravimeter assumed in Bouguer correction, which reduces free-air anomaly.

In both cases, terrain correction is added to Bouguer anomaly.

2.6.3. Variation with time

2.6.3.1. Earth and ocean tides

The solid Earth responds to the pull of the Sun and the Moon just like the oceans, but movements are much smaller. The Sun and the Moon also pull on the gravimeter and its parts. These effects are large enough to affect gravity readings (**Figure 22**). Changes in observed
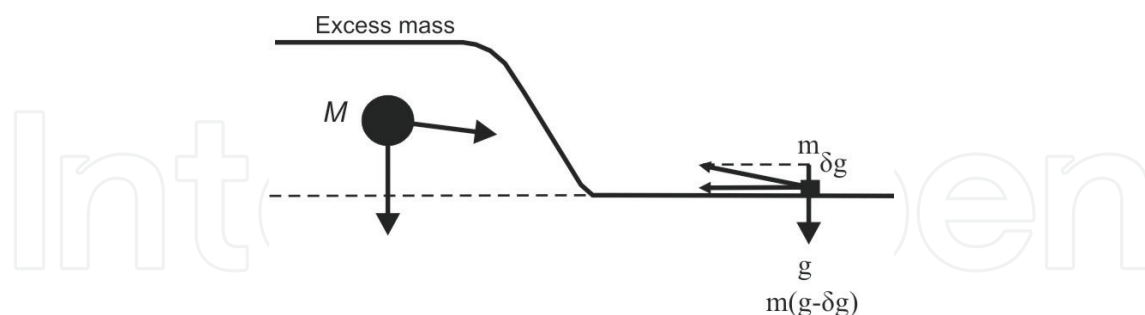
Figure 19. Terrain effect.

Figure 20. Terrain effect.
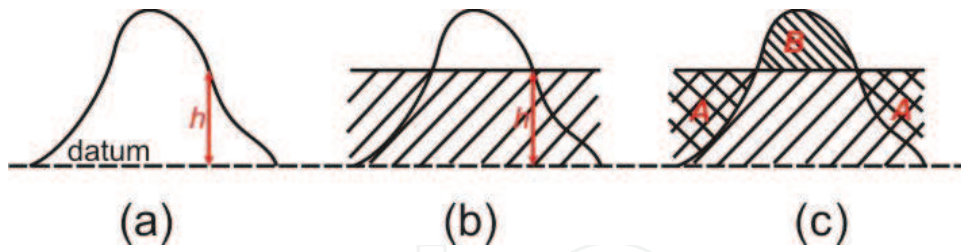
Figure 21. Examples of terrain correction. (a) Gravity station at elevation *h* above geoid. (b) Infinite rock mass assumed for Bouguer correction. (c) Terrain correction compensates for error *A* in *BC* and also *B*.
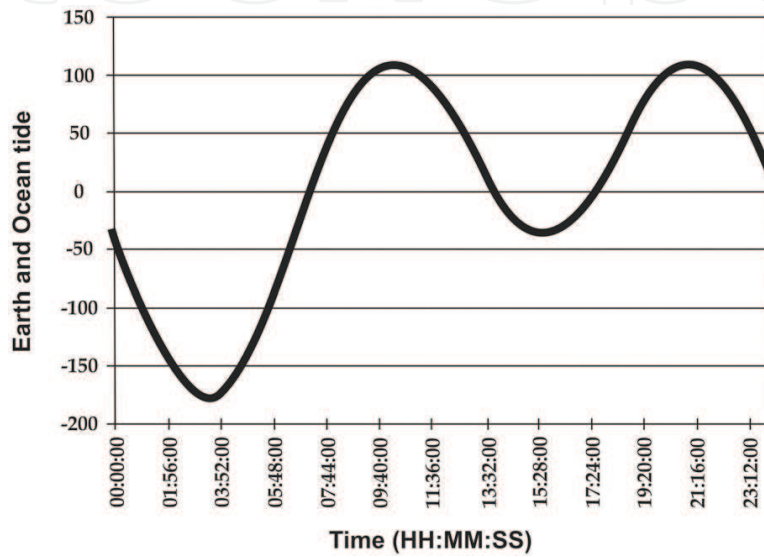
Figure 22. An example of earth tide and ocean load tide effects in µGal at a gravity station in Unzen volcano (southwestern Japan) on August 11th, 1999 using GOTIC2 computer code [7, 9].

gravity due to "tides" occur with periods of 12 h or so. Earth tide effects can be controlled by repeated readings at same station in same way as instrument drift.

Precipitation and atmospheric pressure: These effects can be significant in a microgravity survey. It is recommended to measure gravity in a stable weather condition (on the same day, for example).

2.7. Bouguer anomaly

The Bouguer anomaly (Dg_B) is the difference between the observed value (g_{obs}), properly corrected, and a value at a given base station (g_{base}), such that:

$$\Delta g_B = g_{base} + \sum(\text{corr}) - g_{obs} \tag{5}$$

with

$$\sum(\text{corr}) = \delta g_L + (\delta g_F - \delta g_B) + \delta g_{TC} - \delta g_D \tag{6}$$

Measured gravity data
Gravity tide correction   Correction for solar and lunar mass
Correction for instrumental   Correction for altitude from a ground surface
Drift correction   Correction for the drift of gravity meter
Gravity value at measurement
Topographic correction   Correction for near field topographic mass attraction
Bouguer correction   Correction for near field mass attraction
Free air correction   Correction for gravity difference due to the difference from measurement point the datum altitude
Latitude correction   Correction for the normal gravity
Atmospheric correction   Correction for atmospheric mass attraction
Gravity anomaly distribution (random data)
Complement   Complete random data turn to grid data
Gravity anomaly distribution (grid data)
Fourier analysis (model)
Subsurface density structure   To obtain the target underground density structure based on spectral analysis, filter operation and model calculation.
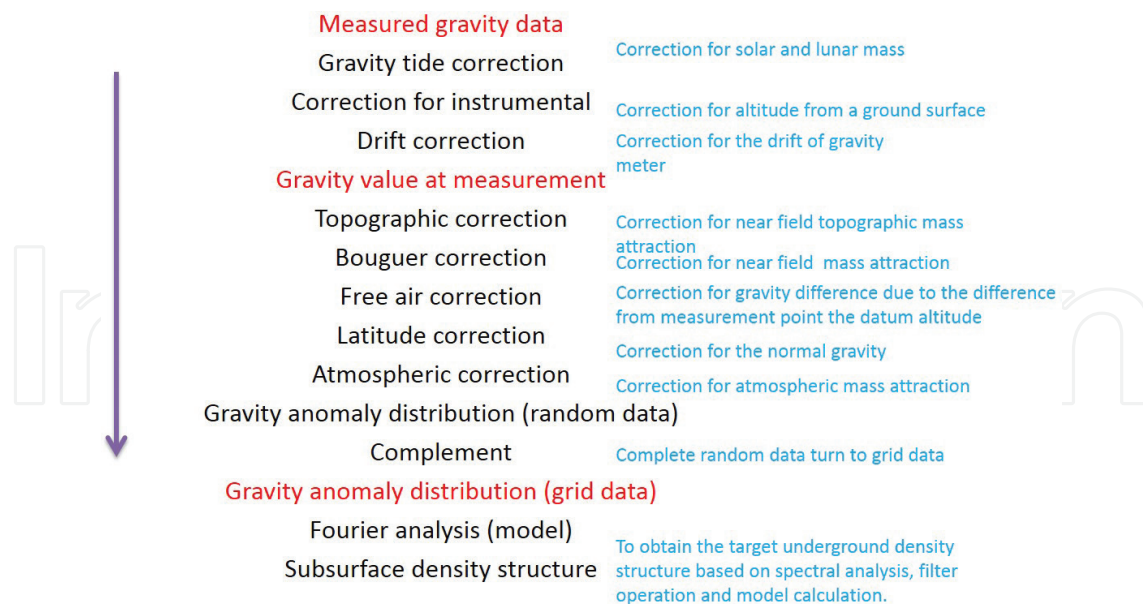
Figure 23. Flow chart of gravity data processing and analysis.

where the subscripts refer to the following corrections: L: latitude; F: free-air; B: Bouguer; TC: terrain correction; and D: drift (including the Earth tides).

Figure 23 shows the different steps for gravity data processing.

3. Applications of gravity method in geosciences with case studies

Gravity can be used for: (1) regional surveys and (2) local surveys. These two cases depend on the scale of the geologic target under the study. For fault and regional geological surveys, we use a regional gravity survey with a large grid size. However, for local geological studies such as cavity investigations, active fault detection or local geological features, we use more dense gravity surveys with a small grid size and small spacing between gravity stations.

3.1. Geology and structural geology

Gravity data can give us much information about the subsurface geological structures such as faults, rock intrusions, dykes, and sills. We can also study basin structure, grabens, horts, and salt intrusion all of which are very important in oil and gas exploration. The most important physical property is rock density, and density contrast between the different rocks will create gravity anomalies which are easy to detect if the measured gravity data are good enough (**Figure 24**). Gravity measurements are very sensitive to noises such as cars and human activities including walking vibrations from machinery or nearby seismic operations and even earthquakes. The geophysicist and/or user must pay close attention during field measurement in order to get good gravity data.
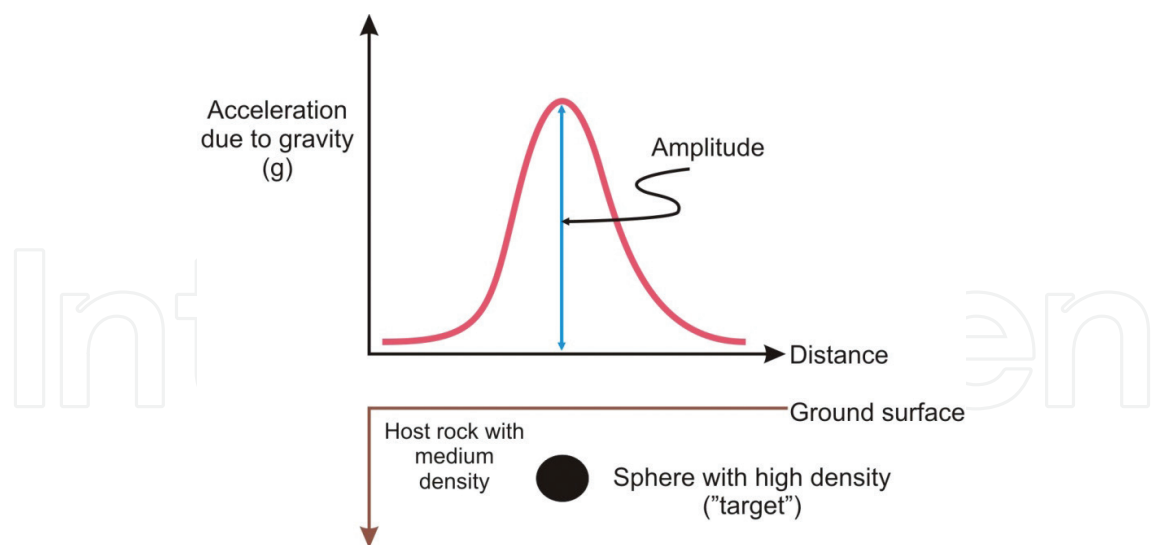
Figure 24. Example of gravity anomaly over a buried sphere with a higher density than the surrounding rocks.

Bouguer anomaly maps contain both regional and residual (local) anomalies (**Figure 25**). Regional anomalies have long wavelengths and are usually due to deep crustal features. A residual (local) anomaly will have a short wavelength and is due to shallower structures.

There are many filtering techniques that can help us to separate the residual and the regional gravity anomalies such as band-pass filters. Power spectrum analysis techniques are also useful in determining the number of geological layers and their depths and can also be used to remove noise from the data.
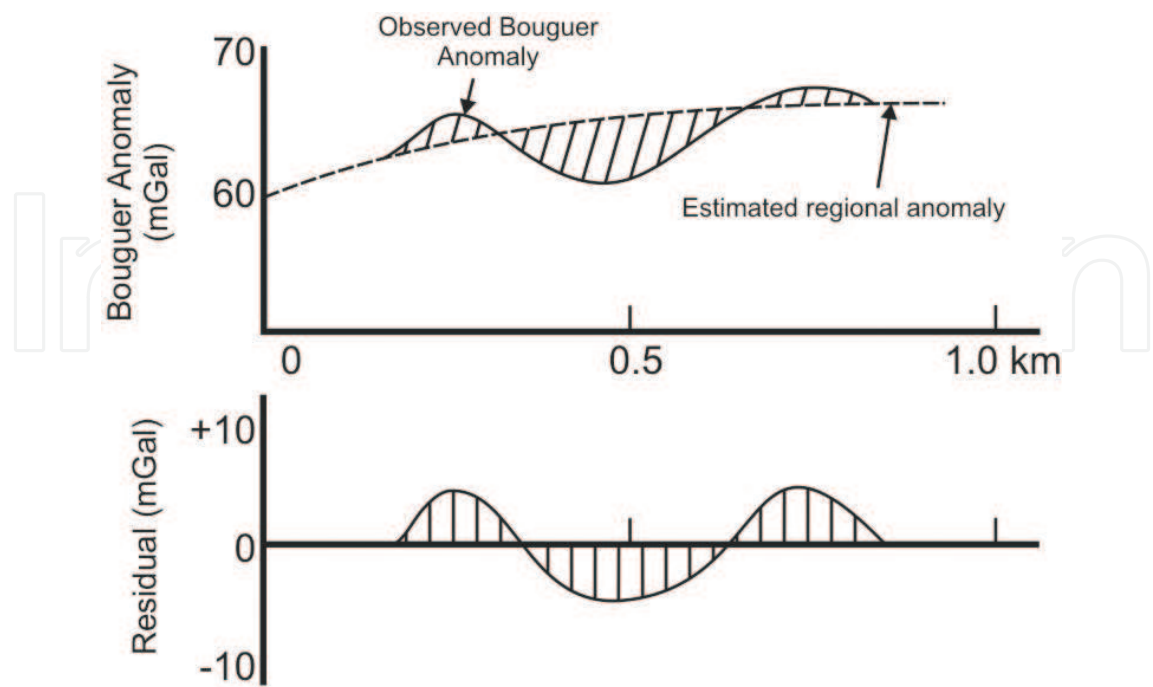

Figure 25. Removal of a residual gravity from a regional profile.

3.1.1. Forward modeling

Figure 26 shows an example of forward modeling of gravity data from Aynak-Logar Valley (Afghanistan) for studying the local geology.

3.1.2. Three-dimensional gravity inversion, case study: Tindouf Basin (Algeria)

The gravity effect of the three-dimensional (3D) density model for Tindouf basin has been computed using GRABLOX-1.7 and BLOXER-1.5 software developed by M. Pirttijärvi, University of Oulu, Finland [11].

The model of study area covers an area of 42,501 km² and was oriented in a north–south direction, extending 269 km in the east–west direction and 157 km in a north–south direction (**Figure 27**). The spatial discretization was 83 grid blocks in the east–west direction ("i" index)
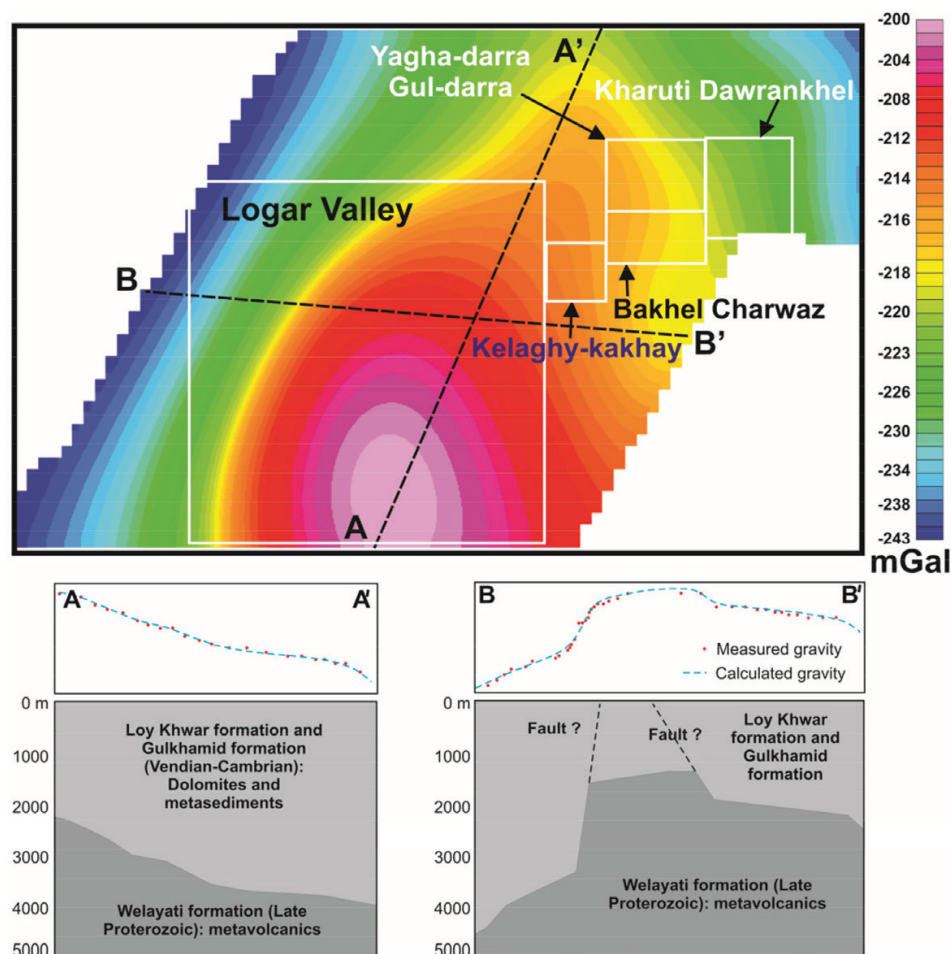
Figure 26. Example of utilization of Bouguer gravity data to construct geological models. Top figure shows Bouguer gravity map at Aynak-Logar valley in Afghanistan with a high gravity anomaly located in southern part of the study area. The figures below show two-dimensional (2D) forward modeling of gravity data using [10] computer code after assigning density values for Loy Khwar and Welayati formations. We can observe a good matching between observed and calculated gravity values. To check the goodness of the geological model, we need to add well data (depth of boundary between the two formations) and use it as control point when creating 2D forward models. [7].

File: Tindouf_data.hei
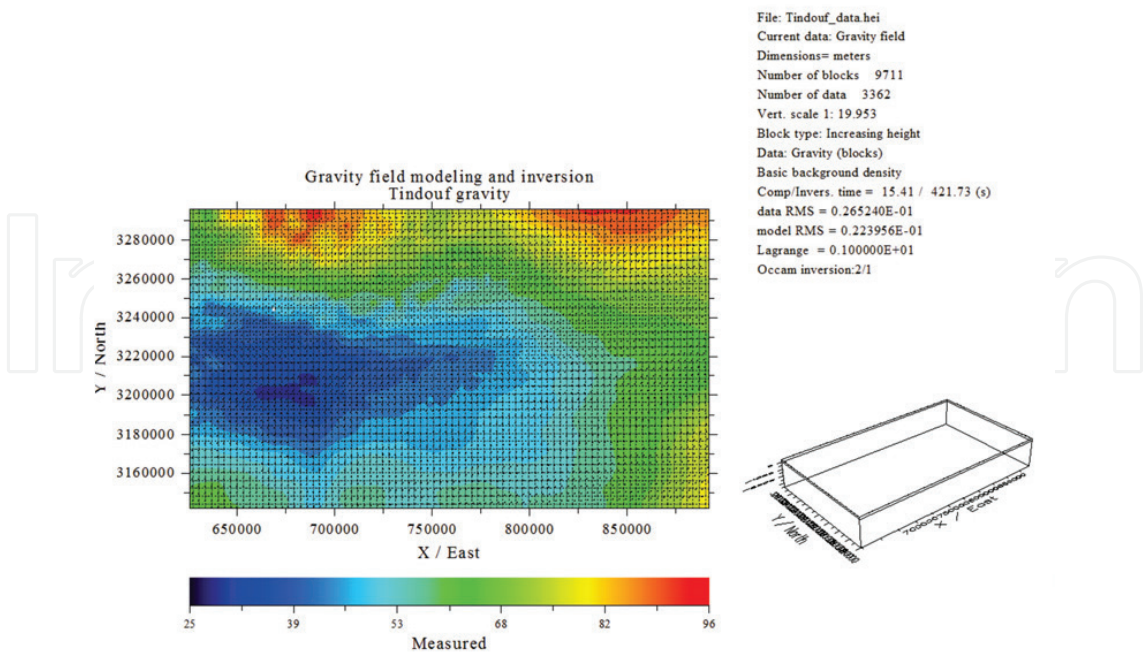Current data: Gravity field
Dimensions= meters
Number of blocks   9711
Number of data   3362
Vert. scale 1: 19.953
Block type: Increasing height
Data: Gravity (blocks)
Basic background density
Comp/Invers. time = 15.41 / 421.73 (s)
data RMS = 0.265240E-01
model RMS = 0.223956E-01
Lagrange = 0.100000E+01
Occam inversion:2/1

Figure 27. Measured Bouguer airborne gravity data of Tindouf basin and the mesh characteristics in preparation for the 3D inversion [7].

and 39 blocks in the north–south direction (''j'' index). In the Z-direction (''k'' index), the model contains three blocks. The model is based on two-layer case: sedimentary layer represented by clays with a density of 2.2 g/cm^3 and a dolerite layer with a density of 2.9 g/cm^3. **Figures 28–32** show the 3D gravity inversion results.

File: Tindouf_model.inp
Current data: Gravity field
Dimensions= meters
Number of blocks   9711
Number of data   3362
Vert. scale 1: 7.943
Block type: Increasing height
Data: Gravity (blocks)
Basic background density
Comp/Invers. time = 15.41 / 421.73 (s)
data RMS = 0.265240E-01
model RMS = 0.223956E-01
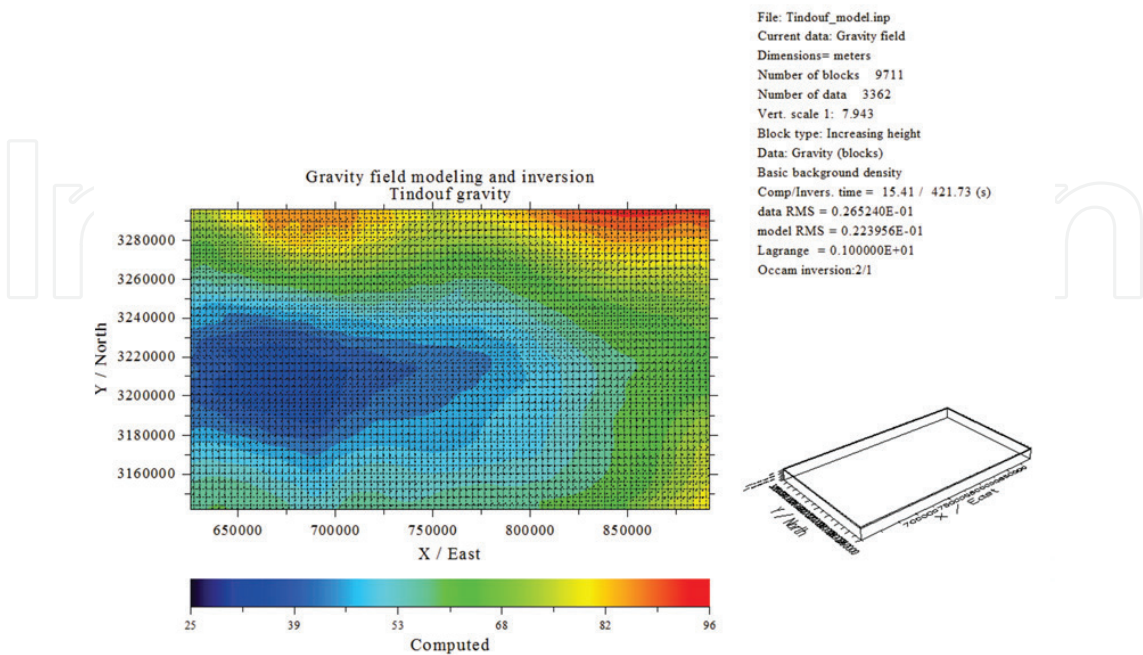Lagrange = 0.100000E+01
Occam inversion:2/1

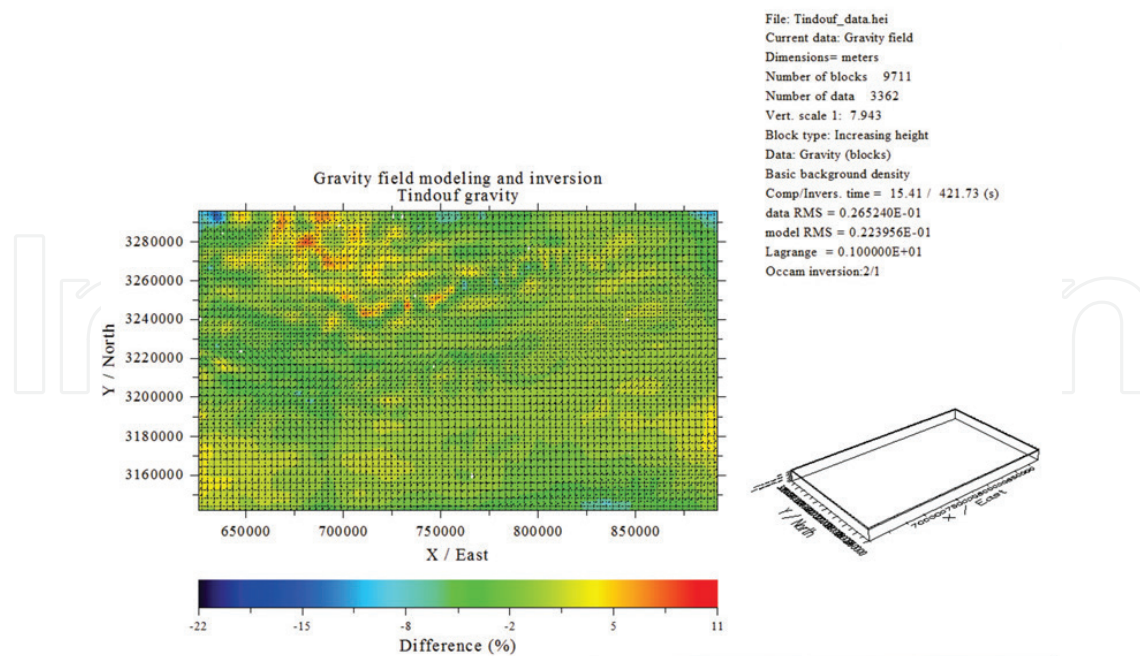**Figure 28.** Computed Bouguer gravity of Tindouf basin [7].

Figure 29. Difference between the computed and the observed Bouguer gravity. Generally, the difference is ranging from 1 to 10% [7].

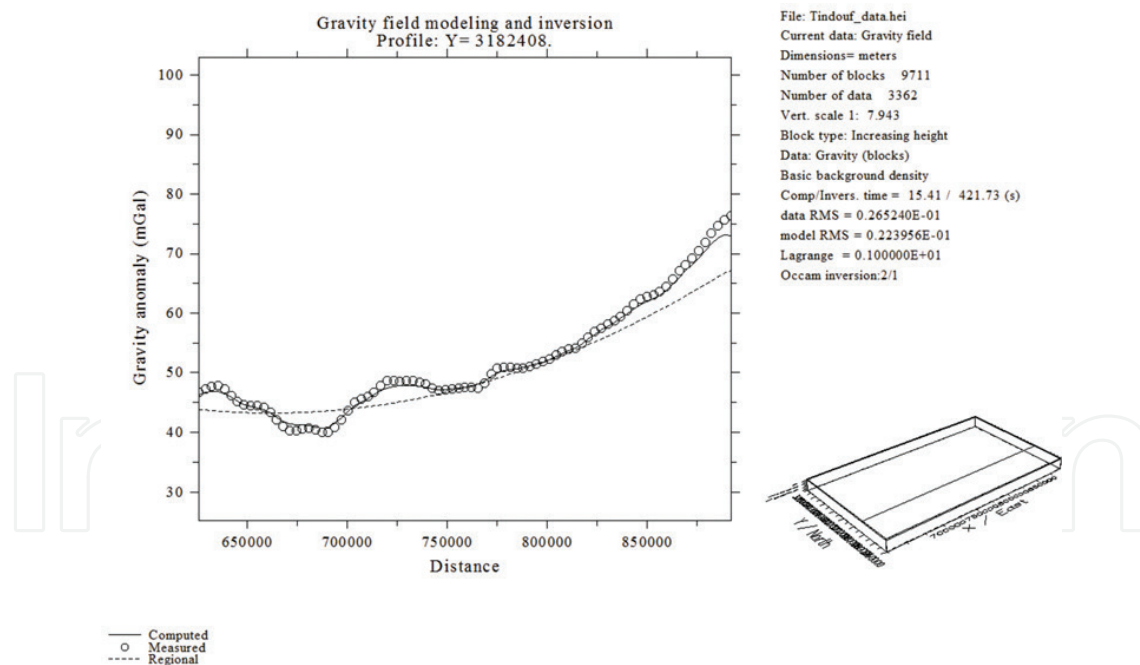**Figure 30.** Comparison plot showing the computed, measured, and regional Bouguer gravity at E-W profile [7].

3.2. Geothermal

Time-lapse gravity surveys at geothermal fields have been going on for at least four decades. The movement of fluids and mass redistribution in geothermal reservoirs are essential for geothermal energy development and its sustainability (**Figure 33**). [12] explained many
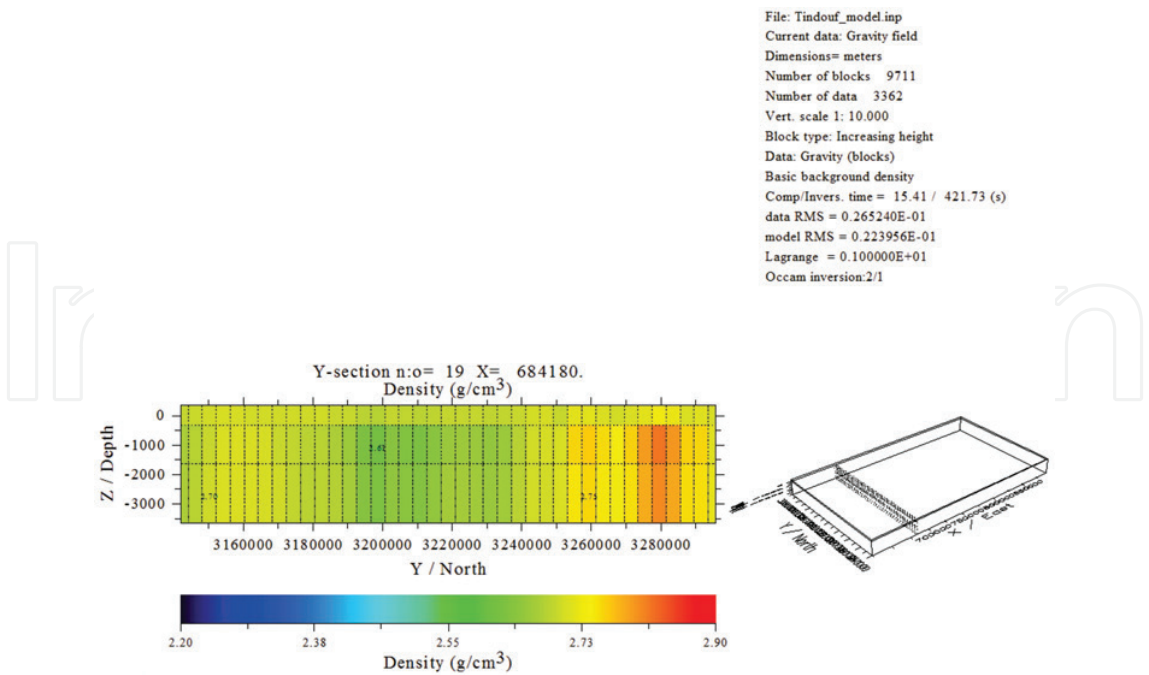
File: Tindouf_model.inp
Current data: Gravity field
Dimensions= meters
Number of blocks   9711
Number of data   3362
Vert. scale 1: 10.000
Block type: Increasing height
Data: Gravity (blocks)
Basic background density
Comp/Invers. time = 15.41 / 421.73 (s)
data RMS = 0.265240E-01
model RMS = 0.223956E-01
Lagrange = 0.100000E+01
Occam inversion:2/1

Figure 31. Section of gravity inversion results at an N-S profile showing high-density rock intrusion (dolerite) at the southern part of the profile [7].

File: Tindouf_model.inp
Current data: Gravity field
Dimensions= meters
Number of blocks   9711
Number of data   3362
Vert. scale 1: 19.953
Block type: Increasing height
Data: Gravity (blocks)
Basic background density
Comp/Invers. time = 15.41 / 421.73 (s)
data RMS = 0.265240E-01
model RMS = 0.223956E-01
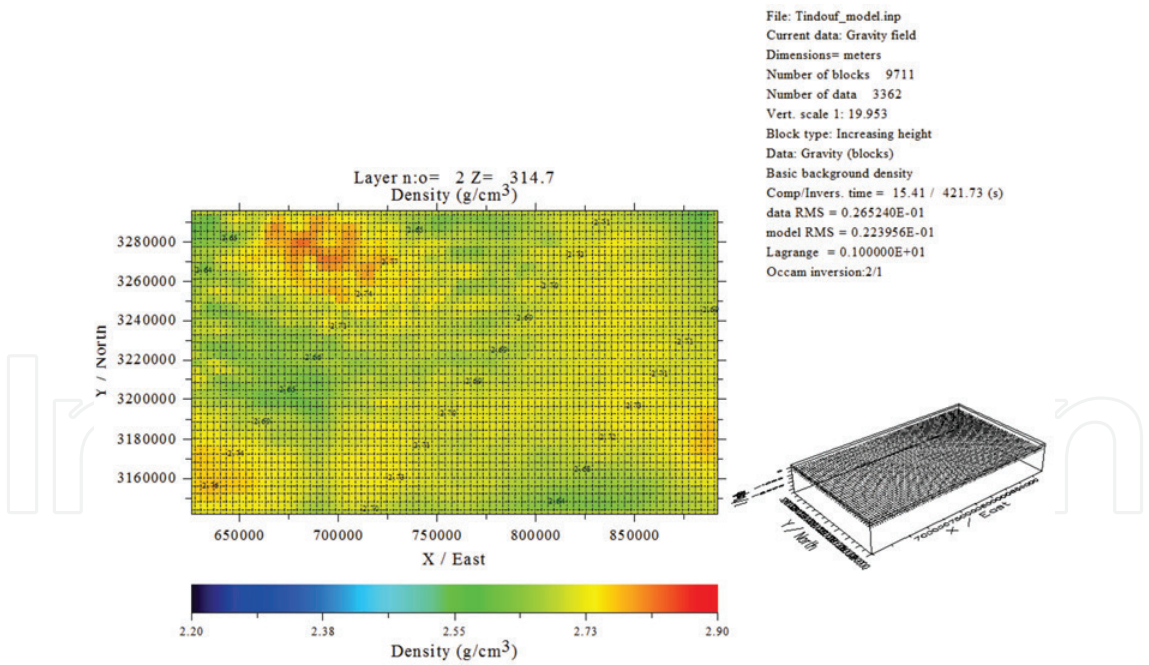Lagrange = 0.100000E+01
Occam inversion:2/1

Figure 32. Top view of gravity inversion results at a depth of 314.7 m (Z is positive downward) showing high-density values in the northwestern part of the study area [7].

possible causes of gravity change at Wairakei geothermal field. Recently, geothermal reservoirs have been monitored with a high-precision hybrid technique (absolute/relative gravity-measurement) [13, 14]. **Figure 34** shows the gravity changes in Obama geothermal field (southwestern Japan).
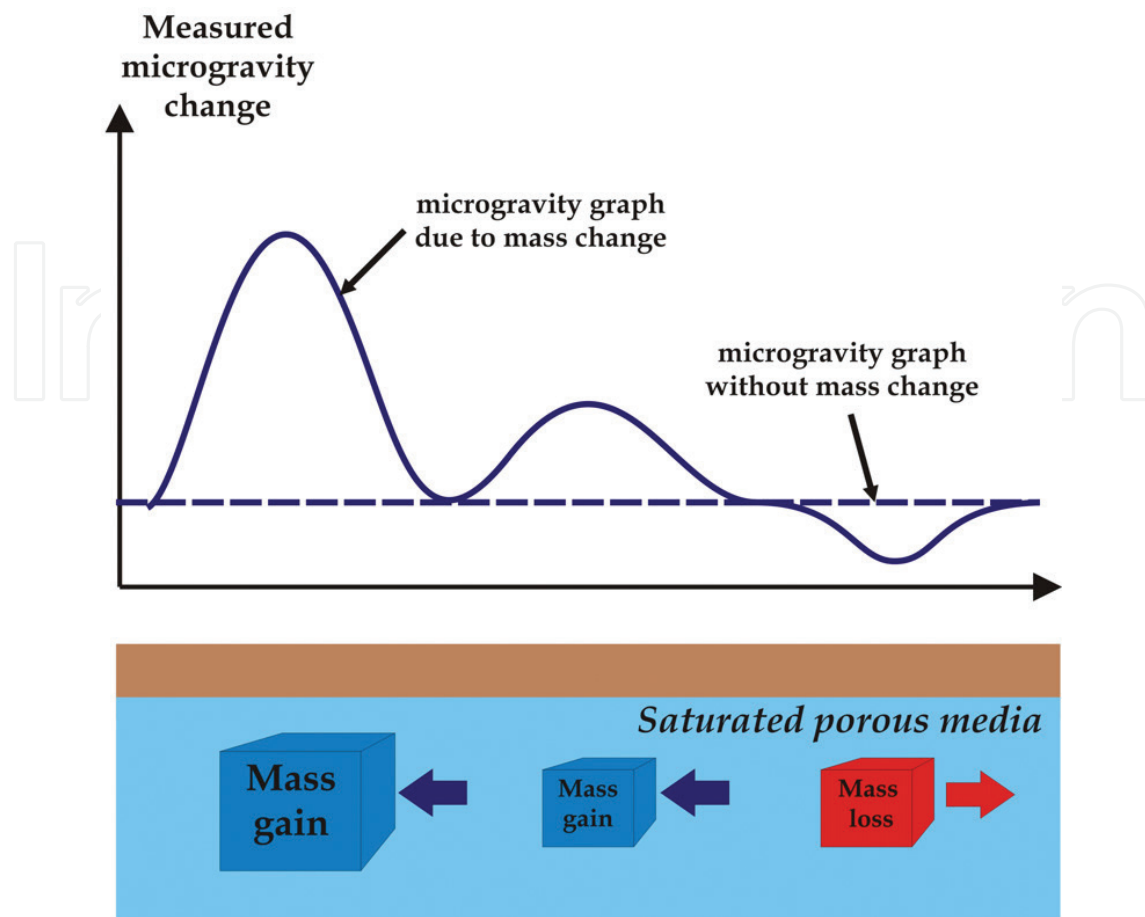
Figure 33. A figure explaining the relation between microgravity changes and mass changes in a geothermal reservoir due to the production and reinjection of waters.

3.3. Hydrogeology

Hydrogeology is perhaps the most complex use of intermediate scale (hour–year) variations in gravity [15]. In the case of horizontal layer (Bouguer slab) of aquifer of thickness h and porosity ϕ, we get a gravity perturbation [16],

$$\Delta g = 2\pi G \rho_{water} \phi h \tag{7}$$

The groundwater level change is calculated after rearranging Eq. (7) as follows:

$$h = \frac{\Delta g}{2\pi G \rho_{water} \phi} \tag{8}$$

Where Δg: gravity change (μGal = 10^{-8} m/s^2), G: universal gravitational constant = 6.673×10^{-11} m^3 kg^{-1} s^{-2}, ρ_{water}: density of groundwater, ϕ: porosity of aquifer, and h: water-level change (m). We assume that the groundwater level variations stem from a shallow aquifer (**Figure 35**); however, there is no bound on aquifer depth in this approximation [5].

Figure 36 shows the evaluation of the required groundwater level changes at the shallow subsurface of Unzen volcano (southwestern Japan) calculated using Eq. (8). The maximum values of water-level change are in the range of several meters.
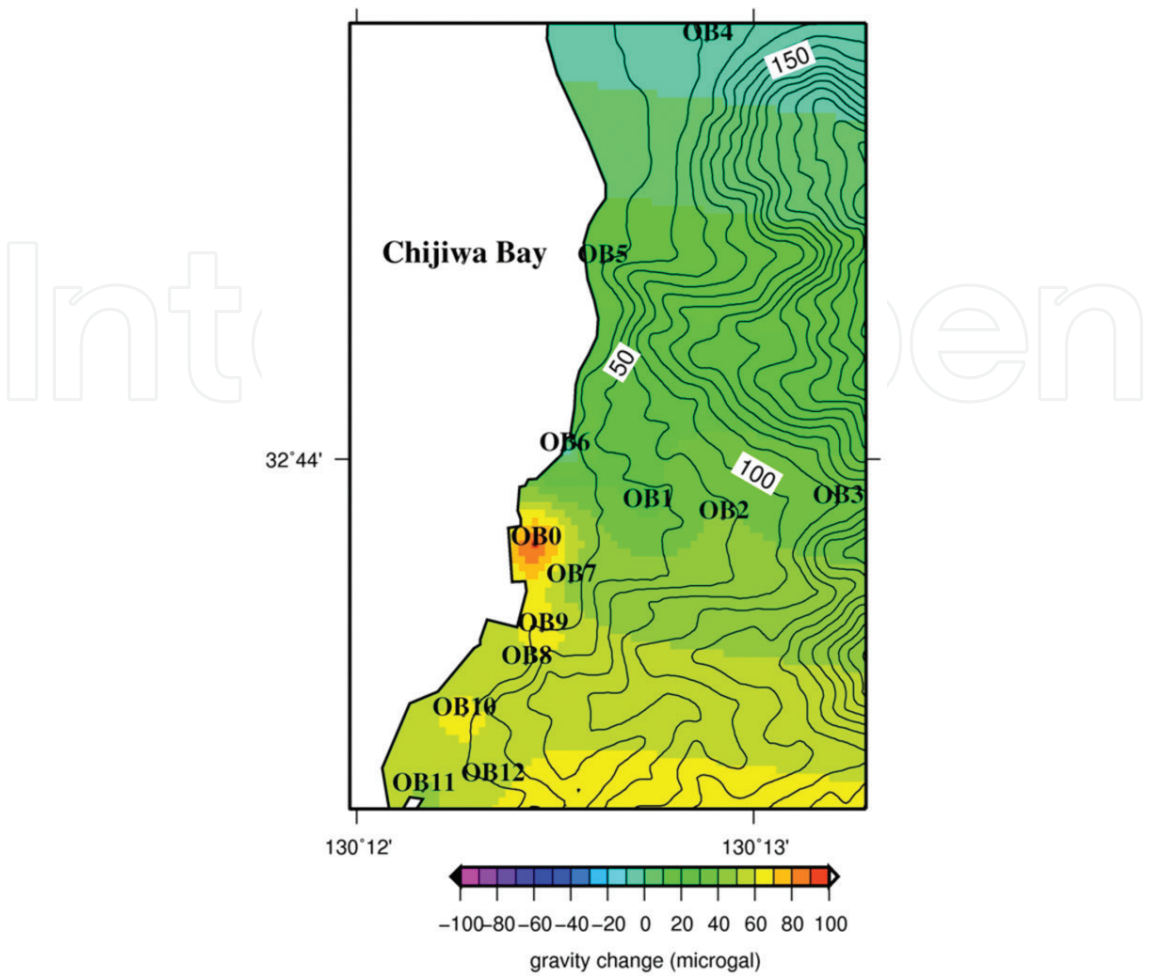
Figure 34. Microgravity changes over the Obama geothermal field (southwestern Japan) from 2003 to 2004. The positive increase of microgravity is interpreted as an excess of mass in the geothermal reservoir [3].
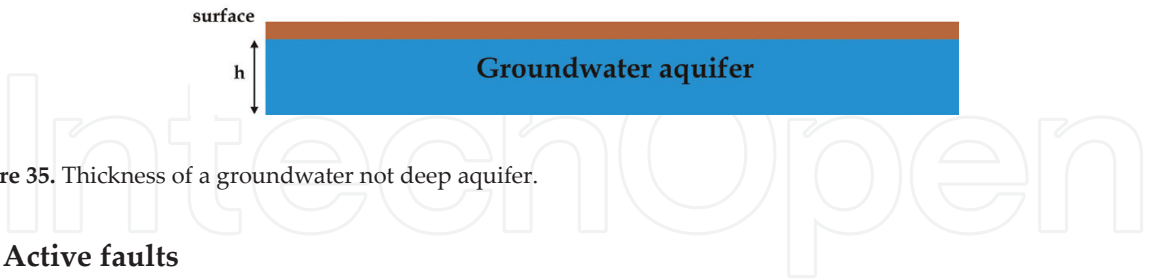

Figure 35. Thickness of a groundwater not deep aquifer.

3.4. Active faults

Gravity method can detect fault zones especially if there is vertical displacement and there is density contrast between the geological layers as shown in **Figure 37**.

3.5. Volcanology

Gravity surveys are very important in monitoring volcanic activity and studying hydrothermal activity beneath volcanoes [5]. **Figure 38** shows the two-may measurements of microgravity in volcanic regions. **Figure 39** explains the different corrections necessary to calculate the residual gravity.
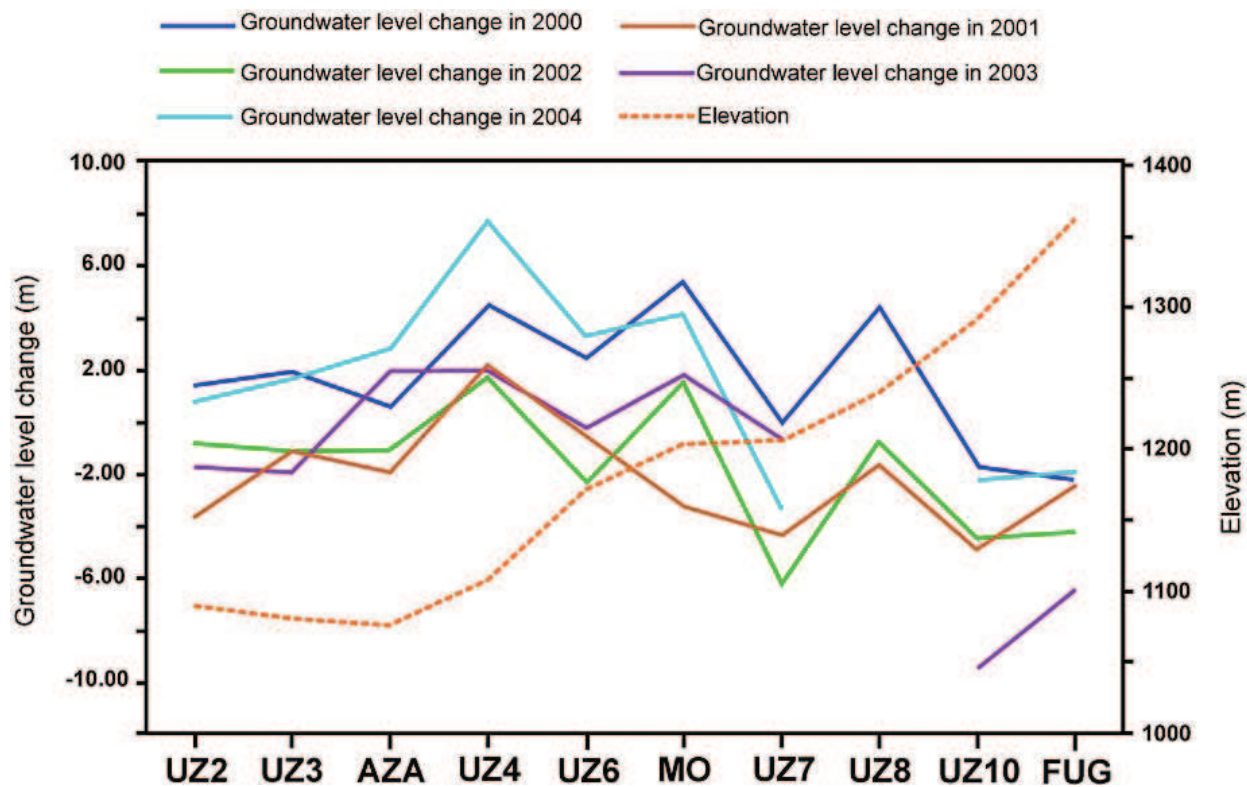
Figure 36. Change of groundwater level with 20% of porosity and topographic elevation along the path crossing stations UZ2 to Fugen microgravity stations in Unzen volcano (Nagasaki prefecture, southwestern Japan). The right vertical axis represents the elevation in meters. The left vertical axis represents the required groundwater level changes in meters [5].
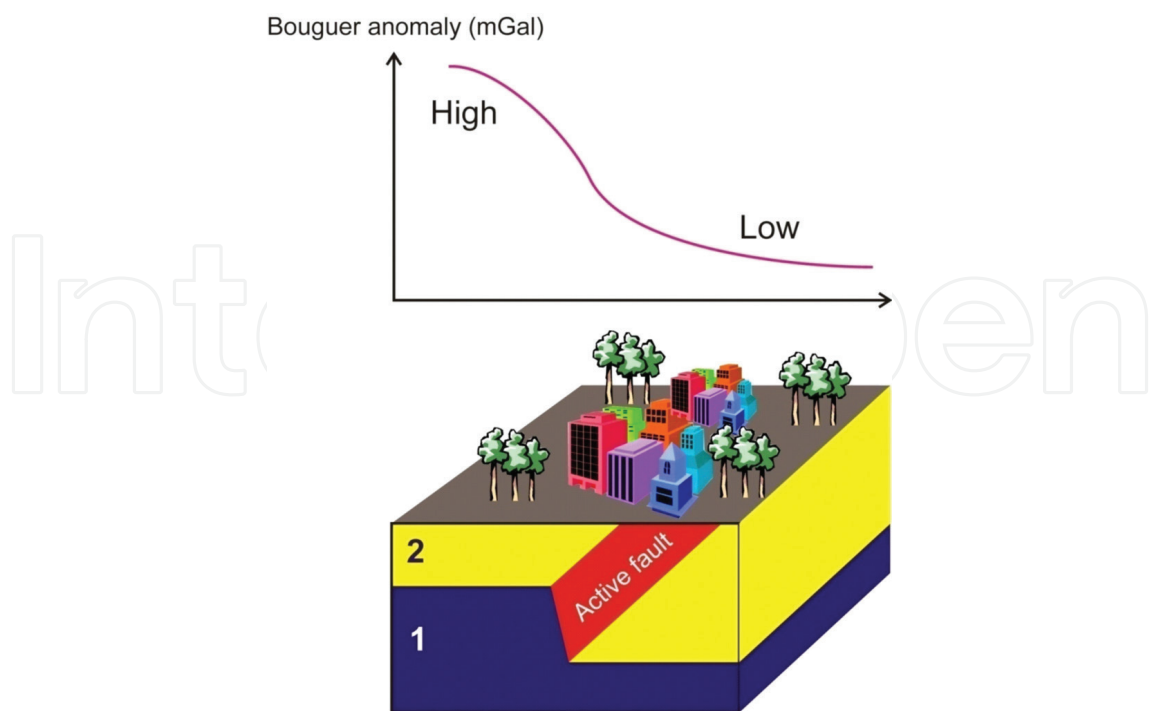

Figure 37. Bouguer gravity anomaly over a normal active fault. Layers 1 and 2 are two geological layers. Layer 1 has a higher density than layer 2.
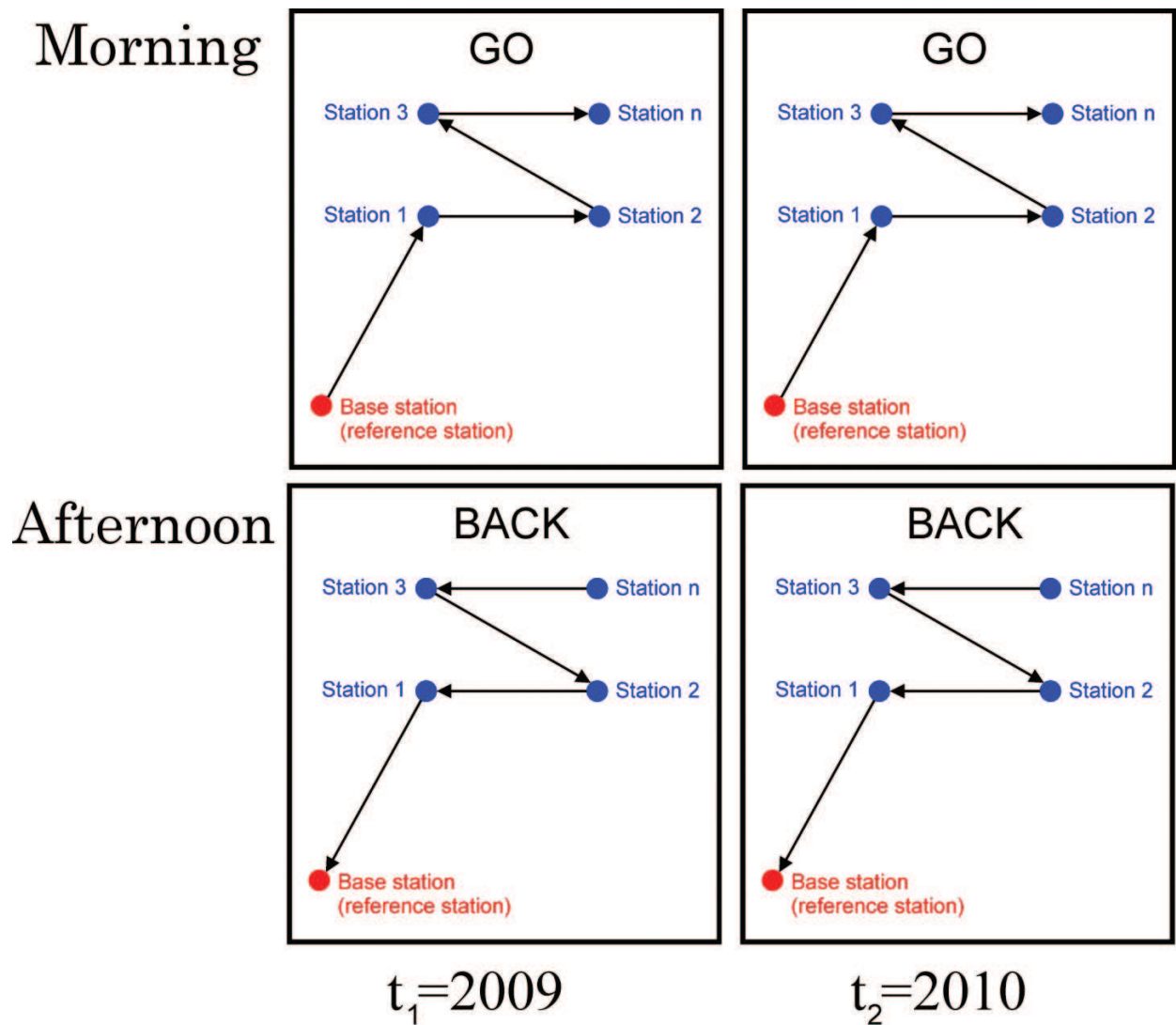
Figure 38. Example of a microgravity monitoring survey at a volcano at different times to monitor volcanic activity.

For gravity surveys in volcanic areas, it is recommended to:

- Use gravity residuals for plotting the gravity changes at a volcano/geothermal field.

- Add the 1-σ error residuals in the same plot of the gravity residuals.

- Use Student's *t*-test to derive indications of statistical relevance of the residual data (to check significant changes at stations).

- Measure gravity in stable weather conditions (i.e., on the same day).

- Minimize operator errors as much as possible by taking the readings in a good way.

3.5.1. Residual gravity calculation

The Residual Gravity at *Station 1* (t_1-t_2) = [(measured gravity at *Station 1* t_2: measured gravity at *Base Station* t_2): (measured gravity at *Station 1* t_1: measured gravity at *Base Station* t_1)].
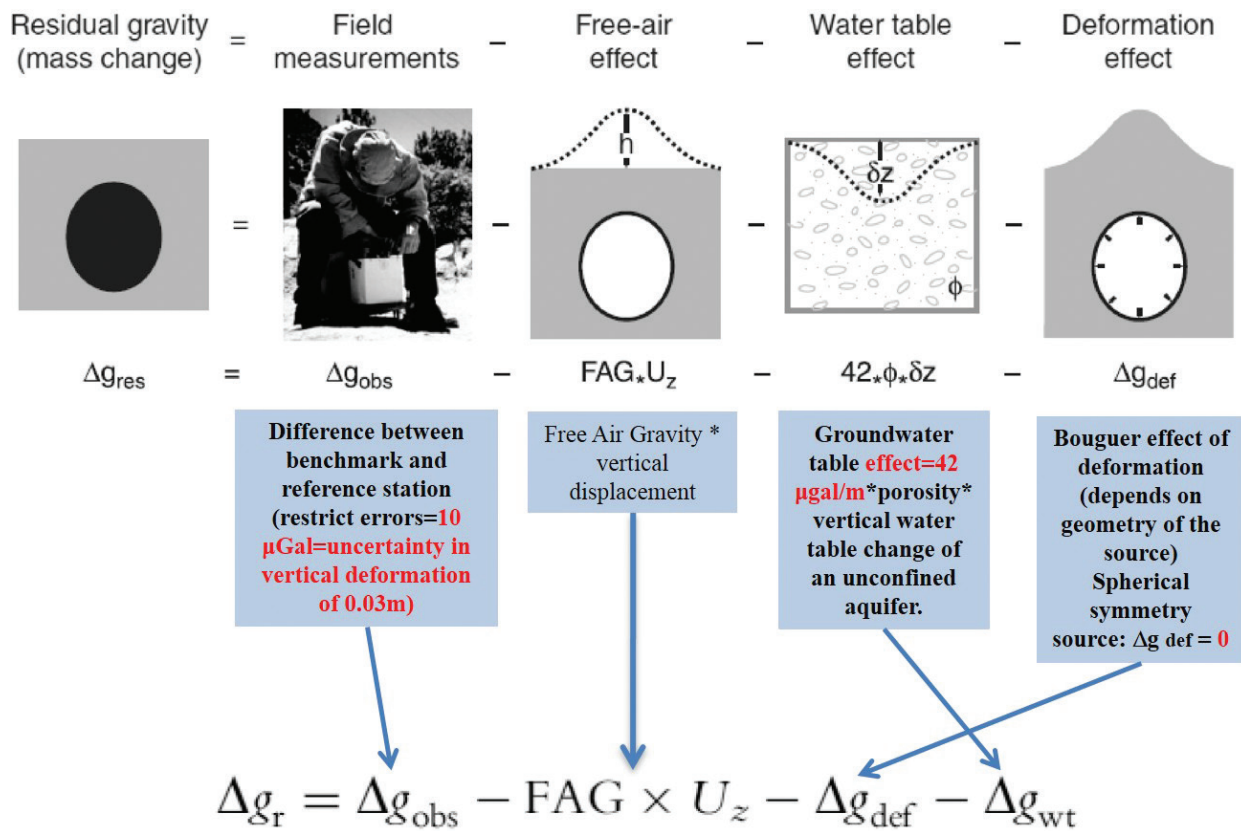
Figure 39. It explains the residual gravity due to residual mass changes at volcanic field [4, 17].

3.5.2. Error datum (1–σ error) calculation

The error for the datum t_1 is as follows:

Error *Station 1* t_1 = sqrt [(error at *Station 1* t_1)^2 + (error at *Base Station* t_1)^2]

For the datum t_2:

Error *Station 1* t_2 = sqrt [(error at *Station 1* t_2)^2 + (error at *Base Station* t_2)^2].

error at Station = sqrt [(drift corrected gravity)go: (drift corrected gravity)back]^2.

3.5.3. Calculation of errors in case of ground deformation

The error of the residual gravity changes (1–σ error residuals) is calculated via:

Residual error *Station 1* t_2 = sqrt [(error *Station 1* t_1)^2 + (error *Station 1* t_2)^2 + (X μGal)^2].

Residual error *Station 1* t_3 = sqrt [(error *Station 1* t_1)^2 + (error *Station 1* t_3)^2 + (2*X μGal)^2].

Residual error *Station 1* t_n = sqrt [(error *Station 1* t_1)^2 + (error *Station 1* t_n)^2 + ((*n*−1)*X μGal)^2].

X μGal is Propagated Error Uncertainty (i.e., deformation effect).

4. Interpretation techniques

In general, we have three categories of interpretation techniques of gravity data: (1) gradient interpretation techniques based on the derivatives of the gravity field, (2) forward modeling of gravity data, and (3) inversion techniques of gravity data in 2D and 3D.

There are many gravity gradient methods developed for detecting fault structures, intrusive high-density bodies, and geological boundaries. Each technique has some advantages for specific geological investigations. In **Table 2**, we summarized these methods, which are very powerful for investigating geological structures as applied to real gravity field data [18–22].

For 2D and 3D modeling and inversion techniques using gravity data, there are many available computer codes and also computer software developed by commercial companies. For more details about these inversion methods and computer codes, you can check these publications [23–26].

Method	Equation	Reference	Advantages
Analytic signal	$AS(x, y) = \sqrt{\left(\frac{\partial P}{\partial x}\right)^2 + \left(\frac{\partial P}{\partial y}\right)^2 + \left(\frac{\partial P}{\partial z}\right)^2}$	[27]	
Tilt derivative	$TDR = \tan^{-1}\left\{\frac{\frac{\partial P}{\partial z}}{\sqrt{\left(\frac{\partial P}{\partial x}\right)^2 + \left(\frac{\partial P}{\partial y}\right)^2}}\right\}.$	[28]	Useful in enhancing and sharpening the potential field anomalies. The zero contour line located on or close to a contact.
Horizontal gradient	$HG = \sqrt{\left(\frac{\partial g}{\partial x}\right)^2 + \left(\frac{\partial g}{\partial y}\right)^2}$	[29]	Least susceptible to noise in the data because it requires only the calculation of the two first-order horizontal derivatives of the field. The method is also robust in delineating both shallow and deep sources.
Euler deconvolution	$(x - x_o)\frac{\partial M}{\partial x} + (y - y_o)\frac{\partial M}{\partial y} + (z - z_o)\frac{\partial M}{\partial z} = n(\beta - M)$	[30]	Assign structural index (0 for fault, 1 for contact, and 2 for a sphere) Help us in detecting linear fault structures and their depths

Table 2. Example of some gravity gradient interpretation methods.

5. Gravity gradiometry

In the last decade, there has been a new way of measuring gravity developed, not only one component as previous conventional gravity field in the vertical direction g_z, but also full
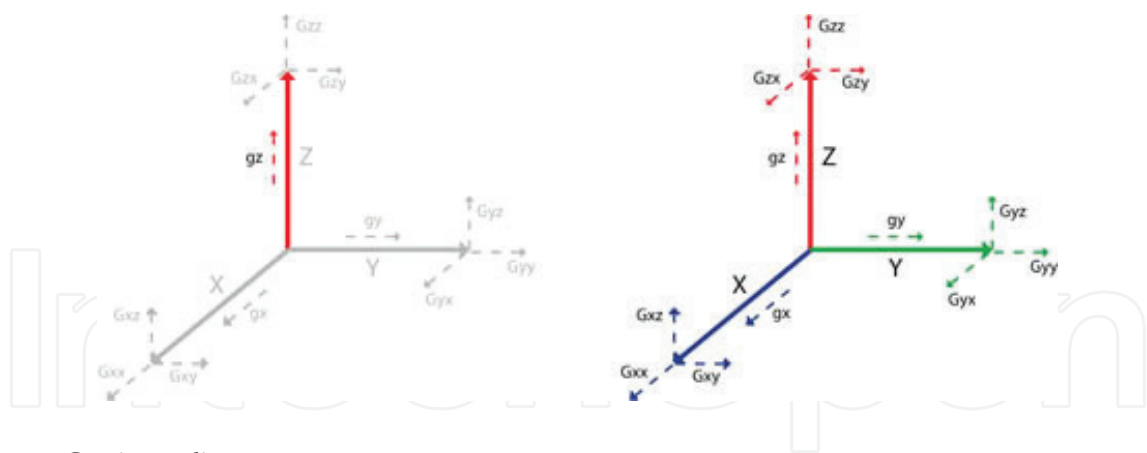
Figure 40. Gravity gradiometry tensors.

tensor gravity gradiometry for all components of the gravity as shown in **Figure 40**. This feature makes the gravity gradient anomaly more localized to the geological source than the gravity anomaly.

6. Gravity data and software

There are many computer programs and codes (**Table 3**) developed by commercial companies or university researchers for gravity data analysis (data filters, data preprocessing, 2D/3D modeling, and 2D/3D inversion).

Software/Code	Link (website)	Capability
PyGMI	http://patrick-cole.github.io/pygmi/index.html#	3D gravity modeling
International Gravimetric Bureau	http://bgi.omp.obs-mip.fr/data-products/Gravity-Databases/Land-Gravity-data	Land and marine gravity data
Fatiando a terra	http://www.fatiando.org/dev/index.html	Modeling and inversion of gravity data
UBC Geophysical Inversion Facility	https://gif.eos.ubc.ca/software/main_programs	Modeling and inversion of gravity data
Geosoft Oasis Montaj	http://www.geosoft.com/products/oasis-montaj	Modeling and inversion of gravity data
Petrel, Gravity Magnetic Modeling and Inversion plug-in (Schlumberger)	https://www.ocean.slb.com/en/plug-ins/plugindetails?ProductId=PGDM-B1	Modeling and inversion of gravity data

Table 3. List of accessible data and computer codes/software for gravity modeling and inversion. There are many other available computer codes for modeling and inversion. The reader can search them at international geophysics journal websites.

7. Conclusions

This chapter summarizes in general from the basics of gravity to instruments used for gravity measurement, gravity corrections, and applications of the gravity method in geosciences. As we stated, gravity is used in many fields of geosciences (geology, structural geology, natural resource exploration, mineral resources, volcanology, geothermal, hydrogeology, CO_2 sequestration, ground cavities, and so).

With the recent development of new gravimeters and availability of satellite gravity data (such as GRACE), the gravity method will be applied in many other new fields for monitoring and estimation of mass changes underground at regional scales (e.g., regional intercontinental aquifers). Also integration and coupling of gravity with other geophysical methods such as magnetics, electromagnetics, seismic and satellite radar such as InSAR will help us increase the accuracy of our geological models and decrease uncertainties in seismic and to help us construct robust geomechanical model for underground oil and gas reservoirs.

Finally, the development of computers and application of robust numerical techniques will certainly help geoscientists to construct near-real geological models.

Acknowledgements

A. Appendix

	1st Measurement	2nd Measurement
Station Name		
Station No.		
Altitude	m	
Height	cm	cm
Reading	mGal	mGal
Read Time	sec	
Date	20.. / /	
Time	: :	: :
Earth Tide Correction	mGal	mGal
Data Rejection		
Standard Deviation	mGal	mGal

	1st Measurement	2nd Measurement
Temperature		
Tilt	X arcsec	arcsec
	Y arcsec	arcsec
Operator		
Companion		
Weather		
Wind		
Temperature	℃	℃
Atmospheric Pressure	hPa	hPa

Table A1. Data sheet for gravity measurement using CG-3/CG-3M gravimeters.

B. Appendix

Date:	**20.. / ……./……. (……….)**
Operator's Name:	
Name of the Station:	
Characteristics of the Battery	
Voltages of the Battery (vehicle battery, AC):	(Volts)
Characteristics of the A-10 Absolute Gravimeter before Measurement:	
"Dropper" Temperature:	(°C) at; (°C) at
"Laser" Temperature:	(°C) at; (°C) at
"IB" Temperature:	(°C) at; (°C) at
Voltages of the Ion Pump:	(Volts) at; (Volts) at
Electric Current of the Ion Pump:	(Ampere)
Voltages of the Fringe amplitude:	(Volts)
Voltages of the Superspring Position SSPOS:	(Volts) at; (Volts) at

*SS POS SS ZERO SS SERVO
Please wait 10 min and check again the spring position.

Characteristics of the station of Measurement	
Longitude:	
Latitude:	
Topographic Elevation:	(m)
Polar motion:	

Date:	20.. / ……./……. (……….)
X:	
Y:	
Height:	(cm)
Measured Absolute Gravity:	(μGal)
Weather Conditions (windy, precipitation, cloudy, atmospheric temperature) and Other Remarks (mechanical noise, etc.):	

Table B1. A-10 absolute gravity measurement data sheet.

Author details

Hakim Saibi

Address all correspondence to: saibi.hakim@gmail.com

Department of Geology, College of Science, United Arab Emirates University, Al-Ain, United Arab Emirates

References

[1] Zeng H, Wan T. Clarification of the geophysical definition of a gravity field. Geophysics. 2004;**60**(5):1252-1254

[2] Hunt TM. Gravity changes at Wairakei geothermal field, New Zealand. Geological Society of America Bulletin. 1970;**81**:529-536

[3] Saibi H, Nishijima J, Ehara S. Reservoir monitoring by repeat microgravity measurement at Obama geothermal field, southwestern Japan. Geothermal and Volcanological Research Report of Kyushu University. 2005;**1**(14):27-31

[4] Battaglia M, Gottsmann J, Carbone D, Fermandez J. 4D volcano gravimetry. Geophysics. 2008;**73**(6):WA3-WA18

[5] Saibi H, Gottsmann J, Ehara S. Post-eruptive gravity changes from 1999 to 2004 at Unzen volcano (Japan): A window into shallow aquifer and hydrothermal dynamics. Journal of Volcanology and Geothermal Research. 2010;**191**(1-2):137-147

[6] Reynolds JM. An Introduction to Applied and Environmental Geophysics. John Willey & Sons Edition; New Jersey, USA. 1998. p. 796

[7] Saibi, H. Personal Data

[8] Schmerge D, Francis O. Set standard deviation, repeatability and offset of absolute gravimeter A10-008. Metrologia. 2006;**43**:414-418. DOI: 10.1088/0026-1394/43/5/012

[9] Matsumoto K, Sato T, Takanezawa T, Ooe M. GOTIC2: A program for computation of oceanic tidal loading effect. Journal of the Geodetic Society of Japan. 2001;**47**:243-248

[10] Talwani M, Worzel JL, Landisman M. Rapid gravity computations for two-dimensional bodies with applications to the Mendocino submarine fracture zone. Journal of Geophysical Research. 1959;**64**:49-59

[11] Pirttijärvi M. GRABLOX2. 2014. Available from: https://wiki.oulu.fi/display/~mpi/Gravity+inversion+using+block+model+2. [Accessed: 2017-09-20]

[12] Allis RG, Hunt TM. Analysis of exploitation-induced gravity changes at Wairakei geothermal field. Geothermics. 1986;**51**:1647-1660

[13] Sugihara M, Ishido T. Geothermal reservoir monitoring with a combination of absolute and relative gravimetry. Geophysics. 2008;**73**(6):WA37-WA47

[14] Nishijima J, Saibi H, Sofyan Y, Shimose S,Fujimitsu Y,Ehara S, Fukuda Y, Hasegawa T,Taniguchi M. Reservoir monitoring using hybrid micro-gravity measurements in the Takigami geothermal field, central Kyushu, Japan. In: Proceedings of the World Geothermal Congress; 25-30 April 2010; Bali (Indonesia):2010. p. 1-6

[15] Harnisch G, Harnisch M. Hydrological influences in long gravimetric data series. Journal of Geodynamics. 2006;**41**(1-3):276-287

[16] Crossley D, Xu H, Van Dam T. Comprehensive analysis of 2 years of data from Table Mountain, Colorado. In: Ducame Band Paquet P (eds.) Proceedings of the 13th International Symposium on Earth Tides. Observatoire Royal de Belgique; 1998. p. 659-668.

[17] Gottsmann J, Battaglia M. Deciphering causes of unrest at collapse calderas: Recent advances and future challenges of joint gravimetric and ground deformation studies. In: Gottsmann J, Martí J, editors. Caldera Volcanism: Analysis, Modelling and Response. Elsevier; Amsterdam, Netherlands. 2008. p. 417-446

[18] Saibi H, Nishijima J, Aboud E, Ehara S. Integrated gradient interpretation techniques for 2D and 3D gravity data interpretation. Earth, Planets and Space. 2006;**58**(7):815-821. DOI: 10.1186/BF03351986

[19] Saibi H, Nishijima J, Aboud E, Ehara S. Euler deconvolution of gravity data in geothermal reconnaissance; the Obama geothermal area, Japan. Journal of Exploration Geophysics of Japan. 2006;**59**(3):275-282

[20] Saibi H, Nishijima J, Ehara S. Processing and interpretation of gravity data for the Shimabara peninsula area, South-western Japan. Memoirs of the Faculty of Engineering, Kyushu University. 2006;**66**(2):129-146

[21] Saibi H, Aboud E, Ehara S. Analysis and interpretation of gravity data from the Aluto-Langano geothermal field of Ethiopia. Acta Geophysica. 2012;**60**(2):318-336

[22] Saibi H, Azizi M, Mogren S. Structural investigations of Afghanistan deduced from remote sensing and potential field data. Acta Geophysica. 2016;**64**(4):978-1003 http://link.springer.com/article/10.1515/acgeo-2016-0046

[23] Toushmalani R, Saibi H. Fast 3D inversion of gravity data using Lanczos bidiagonalization method. Arabian Journal of Geosciences. 2015;**8**:4969-4981. DOI: 10.1007/s12517-014-1534-4

[24] Toushmalani R, Saibi H. 3D gravity inversion using Tikhonov regularization. Acta Geophysica. 2015;**63**(4):1044-1065. DOI: 10.1515/acgeo-2015-0029

[25] Farhi W, Boudella A, Saibi H, Bounif MOA. Integration of magnetic, gravity, and well data in imaging subsurface geology in the Ksar Hirane region (Laghouat, Algeria). Journal of African Earth Sciences. 2016;**124**:63-74 http://www.sciencedirect.com/science/article/pii/S1464343X16303077

[26] Bersi M, Saibi H, Chabou MC. Aerogravity and remote sensing observations of an iron deposit in Gara Djebilet, southwestern Algeria. Journal of African Earth Sciences. 2016;**116**:134-150. DOI: 10.1016/j.jafrearsci.2016.01.004 http://www.sciencedirect.com/science/article/pii/S1464343X16300048

[27] Klingele EE, Marson I, Kahle HG. Automatic interpretation of gravity gradiometric data in two dimensions: Vertical gradient. Geophysical Prospecting. 1991;**39**:407-434

[28] Miller HG, Singh V. Potential field tilt – A new concept for location potential field sources. Applied Geophysics. 1994;**32**:213-217

[29] Cordell L, Grauch VJS. Mapping basement magnetization zones from aeromagnetic data in the San Juan Basin, New Mexico, in Hinze, W. J., Ed., the utility of regional gravity and magnetic anomaly maps. Society of Exploration Geophysicists. Oklahoma, USA. 1985:181-197

[30] Reid AB, Allsop JM, Granser H, Millett AJ, Somerton JW. Magnetic interpretation in three dimensions using Euler deconvolution. Geophysics. 1990;**55**(1):80-91